NASA Technical Memorandum 110298
U. S. Army Research Laboratory Technical Report 1288

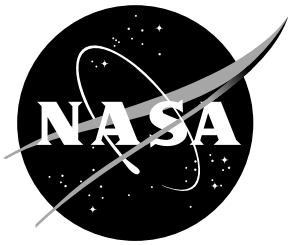

Finite-Element Vibration Analysis and Modal Testing of Graphite Epoxy Tubes and Correlation Between the Data

Barmac K. Taleghani
Vehicle Structures Directorate
U.S. Army Research Laboratory
Langley Research Center, Hampton, Virginia

Richard S. Pappa
Langley Research Center, Hampton, Virginia

November 1996

National Aeronautics and
Space Administration
Langley Research Center
Hampton, Virginia 23681-0001

Finite-Element Vibration Analysis and Modal Testing of Graphite Epoxy Tubes and Correlation Between the Data

B. K. Taleghani* and R. S. Pappa**

NASA Langley Research Center
Hampton, Virginia

SUMMARY

Structural materials in the form of graphite epoxy composites with embedded rubber layers are being used to reduce vibrations in rocket motor tubes. Four filament-wound, graphite epoxy tubes were studied to evaluate the effects of the rubber layer on the modal parameters (natural vibration frequencies, damping, and mode shapes). Tube 1 contained six alternating layers of 30-degree helical wraps and 90-degree hoop wraps. Tube 2 was identical to tube 1 with the addition of an embedded 0.030-inch-thick rubber layer. Tubes 3 and 4 were identical to tubes 1 and 2, respectively, with the addition of a Textron Kelpoxy elastomer. This report compares experimental modal parameters obtained by impact testing with analytical modal parameters obtained by NASTRAN finite-element analysis. Four test modes of tube 1 and five test modes of tube 3 correlate highly with corresponding analytical predictions. Unsatisfactory correlation of test and analysis results occurred for tubes 2 and 4 and these comparisons are not shown. Work is underway to improve the analytical models of these tubes. Test results clearly show that the embedded rubber layers significantly increase structural modal damping as well as decrease natural vibration frequencies.

---

* Army Research Laboratory, VSD
** NASA Langley Research Center

INTRODUCTION

The Army Research Laboratory's Vehicle Structures Directorate (ARL, VSD) has a Technology Program Annex (TPA) agreement with the Army Missile Command (MICOM) to assess the use of layers of rubber to increase damping in filament-wound, graphite epoxy rocket motor tubes. The first phase of the investigation involves modeling and testing four tubes (two with a thin rubber layer at the center of the layup and two without the rubber layer). MICOM fabricated the tubes, performed initial dynamic tests, and delivered their test results and the four tubes to NASA Langley. Additional tests were performed at NASA by suspending the tubes from low-frequency supports, mounting accelerometers, and exciting the tubes with impact loads. Processing the accelerometer responses yielded natural frequencies, mode

shapes, and modal damping. The effects of the rubber layer was then evaluated as was the ability of the analytical models to predict modal characteristics of the tubes.

DESCRIPTION OF TEST ARTICLES

The tubes (figure 1) have a 3.6-inch inside diameter, 41-inch length, and wall thicknesses varying from 0.072 inches to 0.102 inches depending on the layup. The filament winding process used H-IM6 graphite fibers with an anhydride epoxy resin system, wet winding over an aluminum mandrel, and an oven cure in a rotisserie. The cure cycle ramped from an ambient condition to 300 degrees Fahrenheit and held for three hours to ensure complete curing of the matrix. The cylinders were allowed to cool overnight to room temperature, extracted from the mandrel, and then cut to length.

Four tubes (table 1) were manufactured. The baseline tube (tube 1), depicted in figure 2, consisted of alternating layers of 30-degree helical wraps and 90-degree hoop wraps for a total of six layers. Tube 2 is identical to tube 1 with the addition of a 0.030-inch-thick layer of Kevlar-reinforced polyisoprene rubber. The rubber layer was introduced to the cylinder by interrupting the winding process in the middle of the layup. The rubber layer was hand laid, trimmed, and seamed to provide a uniform thickness. The filament winding process was then continued to complete the cylinder fabrication. Tube 3 is the same as the tube 1 except the epoxy was modified with elastomeric copolymer particles ranging from 0.01 to 10 microns in diameter. The concentration of the spheres in the epoxy was 5 percent by weight. Tube 4 is the same as tube 2 except for the addition of an elastomer-modified matrix. The previously mentioned cure cycle was used for all four tubes.

MODAL TEST METHOD

Figure 1a shows the test configuration. Each tube hung on soft bungee cords to obtain free-free boundary conditions. Figure 3 shows the 4 excitation positions and 25 accelerometer positions used in each test. Frequency response functions (FRFs) were measured with impact excitation using a commercial “modal testing” hammer; i.e., a hammer with an integral force gauge. Standard test procedures generated the FRFs with exponential response windowing and 5 ensemble averages. The data-analysis software applied a correction term that removed the increased-damping effects of the exponential window. Each FRF had 512 lines of resolution from 0 to 4096 Hz.

The accelerometer positions used in these tests correspond to those used in previous tests performed at MICOM. They adequately measure radial motion only in the x-z plane passing through the centerline of the tube. Analysis results obtained after testing(discussed in the results section of the report) show that many more sensors are necessary to fully measure the vibration(modal) characteristics of the tubes up to 2000 Hz.

Figure 4 shows sample FRFs for each of the four tubes. These data are driving-point FRFs of each tube at test point 15Z (i.e., at location 15 in the z direction). A driving-point FRF is one in which the excitation and response occur at the same location and in the same direction. The data are of high quality based on the smoothness of the curves and the regularity of the driving-point phase angles (always between 0 and 180 degrees). A count of the resonant peaks shows that there are at least 20 modes from 0 to 4096 Hz.

The accelerometer positions used in these tests correspond to those used in previous tests performed at MICOM. They adequately measure radial motion only in x-z plane passing through the centerline of the tube. Analysis results obtained after testing (discussed in the results section of this report) show that many more sensors are necessary to fully measure the vibration (modal) characteristics of the tubes up to 2000 Hz.

The Eigensystem Realization Algorithm (ERA) (refs. 1 and 2) identified structural modal parameters (natural frequencies, damping, and mode shapes) from the FRFs. ERA is a multiple-input, multiple-output, time-domain technique which analyzes free-decay data or impulse response functions derived by inverse Fourier transformation of FRFs. The FRFs for each tube were analyzed with ERA in 5 separate analyses as follows: 1) using all 100 FRFs (4 excitations and 25 responses) simultaneously, 2) using the 25 responses for excitation 1X only, 3) using the 25 responses for excitation 15Z only, 4) using the 25 responses for excitation 17Z only, and 5) using the 25 responses for excitation 20Y only. The best result for each mode based on the Consistent-Mode Indicator (CMI) (ref. 1) and visual inspection of mode shapes was selected from among the 5 analyses of each tube.

MODAL AND TRANSIENT RESPONSE ANALYSIS

Finite-Element Model

The MSC/NASTRAN (ref. 3) finite-element model is shown in figure 5. The model consisted of 1312 equally spaced quadrilateral elements, 1328 nodes, and 7968 degrees of freedom. The CQUAD4 isoparametric membrane-bending plate element was used to model the tubes. The model incorporated 16 elements around the circumference and 83 elements along the length. Lumped masses were added as individual point masses located at designated nodes of the finite-element model to account for the weight of the instrumentation (figure 6). As shown in figure 6, 3 triple-axis accelerometers (weighing 22 grams each) were located at the ends of the tube, (b) 15 single-axis accelerometers (weighing 2 grams each) were placed 5 inches apart on each side of the longitudinal axis of the tubes, and (c) 1 single-axis accelerometer was located on top. Accelerometers were modeled as point masses and were not offset from the structural nodes. The CONM2 NASTRAN mass element was used for the point masses.

The Integrated Design Engineering Analysis Software, I-DEAS, (ref. 4) was used for pre-and post-processing. A universal file translator transferred

the mesh information into the NASTRAN environment to create the bulk data deck file for finite-element analysis. Table 2 shows the material properties for the analysis. A NASTRAN MAT8 material card defined orthotropic material properties for isoparametric shell elements. Lacking precise knowledge of the constituent materials, the authors used data given by Tsai (ref. 5). The density in table 2 is the weight of the tube divided by the volume of the tube. A separate material card was developed for the layer of rubber. The rubber properties also appear in table 2.

Eigenvalue Analysis

The analysis of the composite tubes presented here was performed using version 68 of the MSC/NASTRAN commercial finite-element analysis computer code. MSC/NASTRAN Solution Sequence 103 was used to analyze the model. Mode shapes and frequencies were calculated in MSC/NASTRAN using the Lanczos method (ref. 3). It was decided to determine all modes with frequencies up to 2000 Hz.

Direct Transient Response Analysis

Transient response analysis allows for studying and optimizing the effect and the location of the rubber layer within the composite cylinder. The following result is presented to serve as a baseline for future work on investigating the damping effects of the rubber layers in these tubes.

Direct transient response analysis allows the computation of the general dynamic response of a structure. This method performs a numerical integration on the complete coupled equations of motion, as follows:

$$[M]\{\ddot{x}\}+[C]\{\dot{x}\}+[K]\{x\}=\{f\} \qquad (1)$$
$$\{x(0)\}=\{x_0\}$$
$$\{\dot{x}(0)\}=\{0\}$$

where:
$[M]$ = Mass Matrix
$[C]$ = Damping Matrix
$[K]$ = Stiffness matrix
$\{f\}$ = Forcing function
$\{\ddot{x}\}$ = Acceleration vector
$\{\dot{x}\}$ = Velocity vector
$\{x\}$ = Displacement vector
$\{x_0\}$ =Initial displacement vector

The first bending vibration mode of frequency ω was used as an initial displacement condition $\{x_0\}$ of the structure. A FORTRAN program was written to set the nodal displacements in the NASTRAN input data deck equal to a scaled value of the mode shape. A time-displacement plot of one of the degrees of freedom which is located on the top of the tube (node 10374) is shown in figure 7a and 7b.

In NASTRAN, the damping matrix $[C]$ is, in general, comprised of several matrices. In the present situation only the modal damping factors were known from the testing. Therefore, the damping matrix used in direct transient response calculations was:

$$[C] = \frac{g}{\omega}[K] \tag{2}$$

where:
g = twice the modal damping factor

RESULTS

Test Results

Measured frequencies and damping factors are given in table 3. The same set of 15 modes occurs for each tube. The mode designations are as follows:

nB-Z	The nth bending mode in the Z direction.
nBR	The nth breathing mode (n = axial direction half-wave count).
Love	Love modes can be described as ovalization of cross section at right (R-Love) and left (L-Love) ends of the tubes. These modes are discussed in more detail on pg.315 of ref. 6.

Modes with CMI values (ref.1) of at least 80 percent are identified with high accuracy and are highlighted with bold type in table 3. Modes with high Modal Phase Collinearity (MPC) values (ref. 1) exhibit classical normal-mode behavior. Low MPC usually indicates identification inaccuracy rather than physical non-normal mode behavior. Table 3 shows that the tubes with a rubber layer (tubes 2 and 4) have considerably higher material damping than those without the rubber layer (tubes 1 and 3).

Figures 8 through 11 show the experimental mode shapes for tubes 1 through 4, respectively. These wireframe plots show motions only at the 25

accelerometer positions used in the test. The measurements were made mostly in the Z direction (figure 3) and only motion in this direction is understandable. Additional sensors at other circumferential locations are necessary to fully measure the modal characteristics.

Figure 12 shows the numerical correlation of the mode shapes for various pairs of tubes using the Modal Assurance Criterion (MAC) (ref. 7). The size of each rectangle plotted in figure 12 is proportional to the corresponding MAC (0 - 100%). Pairs of modes with MAC values of at least 70 percent are darkened for emphasis. This is an indication that the mode shapes are not affected by the rubber layer.

Analysis Results

Analytical and experimental results were obtained for all 4 tubes. NASTRAN analysis determined 32 modes for tubes 1 and 3, and 134 modes for tubes 2 and 4 that included the rigid body modes in the frequency range of 0-2000 Hz. The increase in number of modes for tubes 2 and 4 is attributed to the increase in flexibility of the tubes with the rubber layer.

The correlated mode shapes and corresponding analysis frequencies of tubes 1 and 3 are shown in figure 13a-13e. The modes consist of one Love mode, three bending modes, and one breathing mode. The 3-D modes give a better understanding of the complexity of the dynamic behavior of the tubes. Although a large number of modes were predicted by NASTRAN, no modes correlated for tubes 2 and 4. Since there is no correlation between the experimental data and analytical results for tubes 2 and 4 at the present time, only the correlation results for tube 1 and tube 3 will be discussed.

Correlation of Test and Analysis Results

In this work, the Modal Assurance Criteria (MAC) (ref. 7) was chosen for correlation purposes. Each analysis mode shape is correlated with each test mode shape as follows:

$$MAC = \frac{\left| \sum_{j=1}^{n} \psi_1{}^T(j)\psi_2(j) \right|^2}{\sum_{j=1}^{n}\left(\left(\psi_1{}^T(j)\psi_1(j)\right)\right)\sum_{j=1}^{n}\left(\left(\psi_2{}^T(j)\psi_2(j)\right)\right)} \qquad (3)$$

where:
ψ_1 = Analysis mode shape
ψ_2 = Test mode shape

The MAC is a scalar value between zero and one that measures similarity of mode shapes. Values above 0.70 indicate a good match between the compared modes.

Figures 14a and 14b show the numerical correlation of the mode shapes using MAC for tubes 1 and 3, respectively.The size of each rectangle is proportional to the corresponding MAC (0-100%). Pairs of modes with MAC values of at least 70 percent are darkened for emphasis. The analytical mode shapes which have a MAC value with the test results of at least 70% are plotted in figures 13a-13e. The test mode shapes for all the tubes are plotted in figures 8 - 12. Modes with high correlation include bending, breathing, and Love modes.

For tube 1, four modes matched between test and analysis as shown in table 4. The right side love mode had the best correlation. The measured and predicted frequencies were 688 Hz and 523 Hz, respectively. The mode shape is shown in figure 13a. The MAC value of 0.93 indicated that the mode shapes are practically identical. The first breathing mode had a MAC value of 0.89 and measured and predicted frequencies of 808 Hz and 637 Hz, respectively. The mode shape is shown in figure 13b. The third result was the second breathing mode with measured and predicted frequencies of 845 Hz and 788 Hz, respectively. The mode shape is shown in figure 13c. This result had a correlation factor of 0.91. For the fourth mode, the measured frequency is 2195 Hz and the respective frequencies of the analysis mode is 1926 Hz. The correlation factor is 0.87. This mode is the third bending shown in figure 13d.

Tube 3, had five modes that correlated between the analysis and test results as shown in table 5. The first mode that correlated had a test frequency of 724 Hz and analysis frequency of 523 Hz. The correlation factor or MAC value was 0.94 and the mode was the R-love shown in figure 13a. The next mode that correlated with a MAC value of 0.89 had test and predicted frequencies of 854 Hz and 637 Hz, respectively. The mode type was the first breathing shown in figure 13b. The third mode was the second breathing mode shown in figure 13c. The MAC value of this correlation was 0.89 and the test and predicted frequencies were 893 Hz and 788 Hz. The fourth mode had a test frequency of 1100 Hz and analysis frequency of 1142 Hz. The MAC value was 0.76 and the mode was the third breathing mode shown in figure 13d. The fifth test mode had a frequency of 2305 Hz and analysis frequency of 1926 Hz. The MAC value was 0.82 shown in figure 13e.

Test results were obtained and used to evaluate the effect of the rubber layer. Table 6 shows the comparison of matched mode shapes and their respective frequencies for tube 3 without the rubber layer and tube 4 with the rubber layer. There were 15 modes not including the rigid body modes that matched between these two tubes. The best correlation (with frequencies of 474 Hz and 433 Hz, respectively) was mode 1. The MAC values ranged from 0.99 to 0.61. The largest difference in frequencies occurred between modes no.

12 of tube 3 having a frequency of 2517 Hz and tube 4 having a frequency of 1866 Hz. The frequencies for tube 4 were generally lower than for tube 3 on the other hand damping values in tube 4 were higher than that in tube 3 due to the presence of the rubber layer in table 6. The experimental frequencies and damping values are summarized in table 3.

CONCLUDING REMARKS

This report described test and analysis results obtained for four graphite epoxy missile tubes, two having an embedded layer of rubber. The rubber layer significantly increased the damping of the structure which reduces vibration during operation. Measured modal damping factors (percent of critical damping) of the tubes without the rubber layer were approximately 0.5%, increasing to approximately 2-3% for the tubes with the rubber layer. The embedded rubber layer also caused natural frequencies of the modes to decrease by approximately 10-20%.

Modal tests were performed using 25 accelerometer locations. These accelerometer locations adequately measured the motion only in a single plane passing through the centerline of the tube. Subsequent NASTRAN analytical predictions showed that additional measurement locations are necessary to fully characterize the complex motion of the tubes in the frequency range of interest (0-2000 Hz).

NASTRAN finite-element analysis predicted 26 elastic modes below 2000 for the tubes without the rubber layer (tubes 1 and 3) and 128 elastic modes below 2000 Hz for tubes with the rubber layer (tubes 2 and 4). The large increase in modes is attributed to increased flexibility of the tubes having the rubber layer. Based on the 25 available measurements, 4 of the NASTRAN modes of tube 1 and 5 of the NASTRAN modes of tube 3 correlated highly with the test results. Unsatisfactory test-analysis correlation occurred for all modes of tubes 2 and 4. It may be necessary to perform additional tests with more measurement locations in order to resolve the discepancies between test and analysis due to the complex nature of the (predicted) mode shapes.

REFERENCES

1. Pappa, R. S., Elliott, K. B., Schenk, A, Consistent-Mode Indicator for the Eigensystem Realization Algorithm, J. Guidance, Control, and Dynamics, Vol. 16, No. 5, Sept. 1993, pp. 852-858.

2. Pappa, R. S., Eigensystem Realization Algorithm User's Guide for VAX/VMS Computers, Version 931216, NASA TM-109066, May 1994.

3. MSC/NASTRAN Handbook for Composite Analysis, The MacNeal-Schwendler Corporation, 1993.

4. I-DEAS Test Data Analysis User's Guide, Structural Dynamics Research Corporation, 1990.

5. Tsai, S. W., Composite Design - 1985, Think Composite, Dayton, OH, 1985.

6. Belvin R.D., Formulas For Natural Frequency and Mode Shape, Kreiger Publishing Co., Malabar, FL, 1984.

7. Ewins, D. J., Modal Testing: Theory and Practice, John Wiley and Sons Inc., New York, NY, 1984.

Table 1

Tube Configurations

Tube 1	Alternating layers of 30-degree helical wraps and 90-degree hoop wraps for a total of six layers.
Tube 2	Same as first tube with the addition of a 0.030-inch-thick layer of Kevlar-reinforced polyisoprene rubber.
Tube 3	Same as first tube, except the matrix was modified with an elastomer*.
Tube 4	Same as second tube, except the matrix was modified with an elastomer*.

Matrix formulation for tubes 1 and 2:

1. Shell Epon 826 (diglycidal ether of bisphenol A)	100 grams
2. CIBA GEIGY RD-2 (diluent)	10 grams
3. CIBA GEIGY 906 (nadic methyl anhydride)	90 grams
4. Pacific Anchor chemical company Imicure EMI-24	1.5 grams

* Matrix Formulation for tubes 3 and 4:

1. Shell Epon 826 (diglycidal ether of bisphenol A)	60 grams
2. CIBA GEIGY RD-2 (diluent)	10 grams
3. CIBA GEIGY 906 (nadic methyl anhydride)	90 grams
4. Pacific Anchor chemical company Imicure EMI-24	1.5 grams
5. Textron Kelpoxy G293-100 (75% 828, 25% Acrylonitrile)	40 grams

Table 2.

MATERIAL PROPERTIES

Tube Configuration

Inside radius = 1.841 in

Thickness(without the layer of rubber) = 0.072 in

Tube length = 41 in

Tube weight(without the layer of rubber) = 2.416 lb

Composite structure properties	**Rubber properties**
$E_1 = 29.44 \times 10^6$ psi	$E_1 = 450$ psi
$E_2 = 1.624 \times 10^6$ psi	$E_2 = 450$ psi
$G_{12} = 1.218 \times 10^6$ psi	$G_{12} = 200$ psi
$G_{1z} = 1.218 \times 10^6$ psi	$G_{1z} = 200$ psi
$G_{2z} = 1.218 \times 10^6$ psi	$G_{2z} = 200$ psi
$\nu_{12} = 0.32$	$\nu_{12} = 0.49$
$\rho = 1.9913 \times 10^{-4}$ lb / in^3	$\rho = 0.89 \times 10^{-4}$ lb / in^3

Table 3.
Measured Frequencies and Damping of Tubes 1- 4

(a) TUBE 1

Mode	Natural Frequency, Hz	Damping Factor, %	CMI, %	MPC, %
1B-Z	**459**	**0.26**	**98**	**99**
2B-Z	1158	1.51	9	17
3B-Z	**2195**	**0.63**	**93**	**99**
4B-Z	**2298**	**0.57**	**89**	**97**
5B-Z	**2387**	**0.69**	**90**	**99**
6B-Z	**2542**	**0.78**	**91**	**96**
7B-Z	**2754**	**0.85**	**96**	**98**
R-Love	**688**	**0.55**	**94**	**99**
L-Love	**726**	**0.52**	**97**	**99**
1BR	**808**	**0.20**	**98**	**99**
2BR	**845**	**0.46**	**95**	**98**
3BR	1045	2.53	8	25
4BR	1430	1.84	64	70
5BR	**1964**	**1.60**	**89**	**99**
6BR	2489	1.22	32	65

(b) TUBE 2

Mode	Natural Frequency, Hz	Damping Factor, %	CMI, %	MPC, %
1B-Z	**431**	**0.32**	**98**	**100**
2B-Z	1184	5.08	5	32
3B-Z	1606	3.02	49	88
4B-Z	1674	2.83	74	90
5B-Z	1801	2.77	60	86
6B-Z	1958	2.14	50	96
7B-Z	2229	1.99	17	78
R-Love	555	2.79	67	84
L-Love	**575**	**2.73**	**88**	**93**
1BR	**691**	**3.28**	**89**	**98**
2BR	**741**	**2.27**	**94**	**99**
3BR	911	3.14	47	61
4BR	1377	2.65	72	86
5BR	1745	2.86	28	72
6BR	**2434**	**1.73**	**80**	**94**

(c) TUBE 3

Mode	Natural Frequency, Hz	Damping Factor, %	CMI, %	MPC, %
1B-Z	**474**	**0.26**	**98**	**99**
2B-Z	1178	3.15	23	39
3B-Z	2305	0.29	70	92
4B-Z	**2424**	**0.60**	**88**	**93**
5B-Z	**2517**	**0.63**	**90**	**96**
6B-Z	**2670**	**0.97**	**84**	**92**
7B-Z	**2879**	**0.79**	**96**	**99**
R-Love	**724**	**0.49**	**97**	**99**
L-Love	784	1.02	79	80
1BR	**854**	**0.18**	**97**	**98**
2BR	**893**	**0.69**	**83**	**86**
3BR	1100	1.60	74	77
4BR	1490	2.51	35	38
5BR	**2064**	**1.19**	**93**	**97**
6BR	2600	1.40	63	78

(d) TUBE 4

Mode	Natural Frequency, Hz	Damping Factor, %	CMI, %	MPC, %
1B-Z	**433**	**0.32**	**99**	**100**
2B-Z	1061	1.77	16	20
3B-Z	1675	2.31	38	46
4B-Z	1734	2.39	72	94
5B-Z	1865	2.39	52	90
6B-Z	**2037**	**1.86**	**85**	**97**
7B-Z	2258	0.82	24	46
R-Love	560	3.53	48	92
L-Love	659	2.99	34	83
1BR	**712**	**2.17**	**82**	**97**
2BR	**778**	**1.81**	**95**	**99**
3BR	989	2.88	48	54
4BR	1332	2.06	71	78
5BR	1789	2.08	58	78
6BR	1969	2.11	73	96

Table 4.

COMPARISON OF MATCHED MODE SHAPES
AND THEIR FREQUENCIES FOR TUBE 1.

MAC VALUE	MEASURED FREQUENCY	COMPUTED FREQUENCY	MODE TYPE
0.93	688	523	Right-side Love Fig. 8h / Fig. 13a
0.89	808	637	1st Breathing Fig. 8j / Fig. 13b
0.91	845	788	2nd Breathing Fig. 8k / Fig. 13c
0.87	2195	1926	3rd Bending - Z Fig. 8c / Fig. 13d

Table 5.

COMPARISON OF MATCHED MODE SHAPES
AND THEIR FREQUENCIES FOR TUBE 3.

MAC VALUE	MEASURED FREQUENCY	COMPUTED FREQUENCY	MODE TYPE
0.94	724	523	Right-side Love Fig. 10h / Fig. 13a
0.89	854	637	1st Breathing Fig. 10j / Fig. 13b
0.89	893	788	2nd Breathing Fig. 10k / Fig. 13c
0.76	1100	1142	3rd Breathing Fig. 10I / Fig. 13d
0.82	2305	1926	3rd Bending - Z Fig. 10c / Fig. 13e

Table 6.

COMPARISON OF MATCHED MODE SHAPES
AND THEIR FREQUENCIES FOR TUBE 3 vs. TUBE 4

MAC VALUE	MEASURED FREQUENCY FOR TUBE 3 (without rubber layer)	MEASURED FREQUENCY FOR TUBE 4 (with rubber layer)
0.99	474	433
0.92	724	561
0.85	784	659
0.76	854	711
0.74	893	778
0.74	1490	1333
0.61	2305	1734
0.80	2424	1789
0.84	2517	1866
0.85	2670	2038
0.75	2879	2258

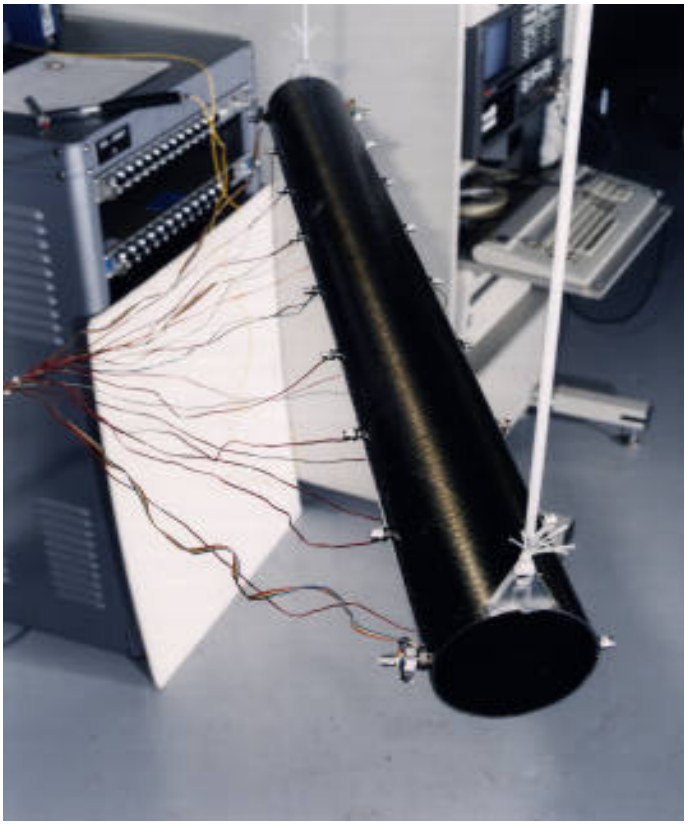

(a) Test Article

(All 4 tubes are similar in appearance)

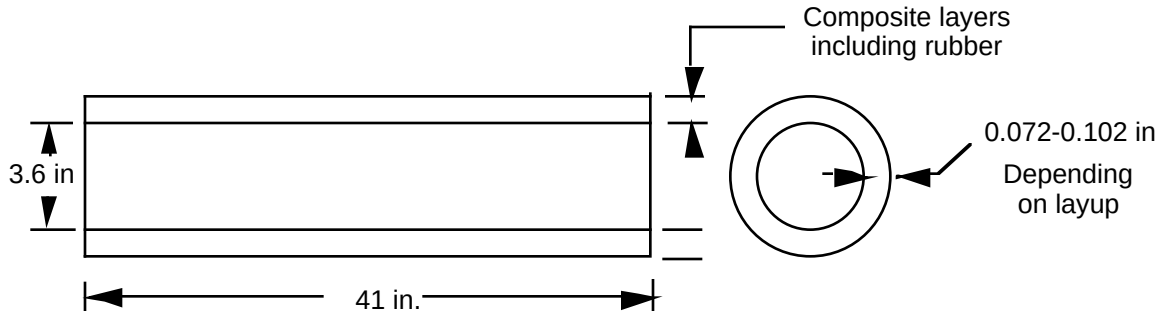

(b) Geometry

Figure 1. Graphite epoxy tubes

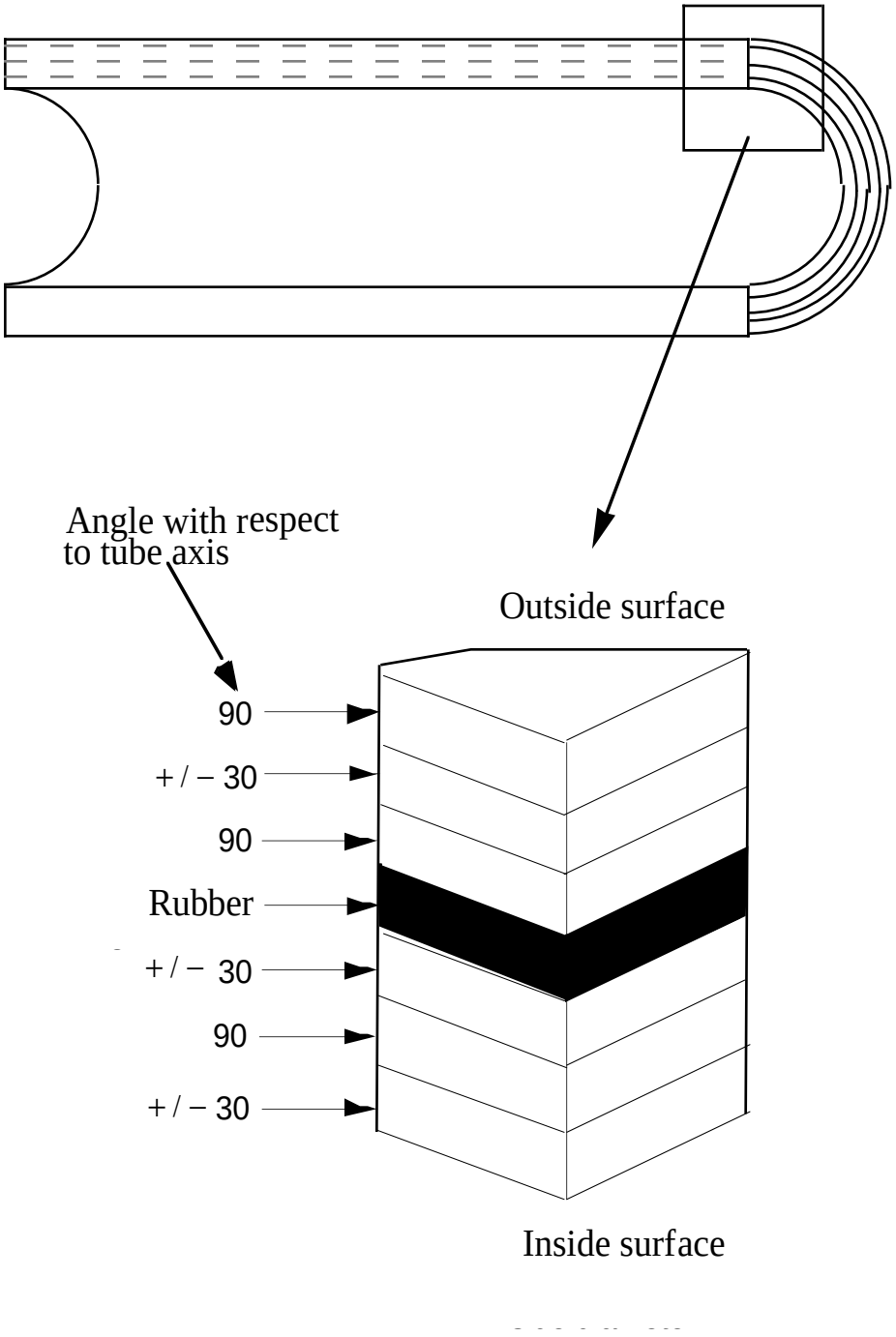

Figure 2. Composite layup

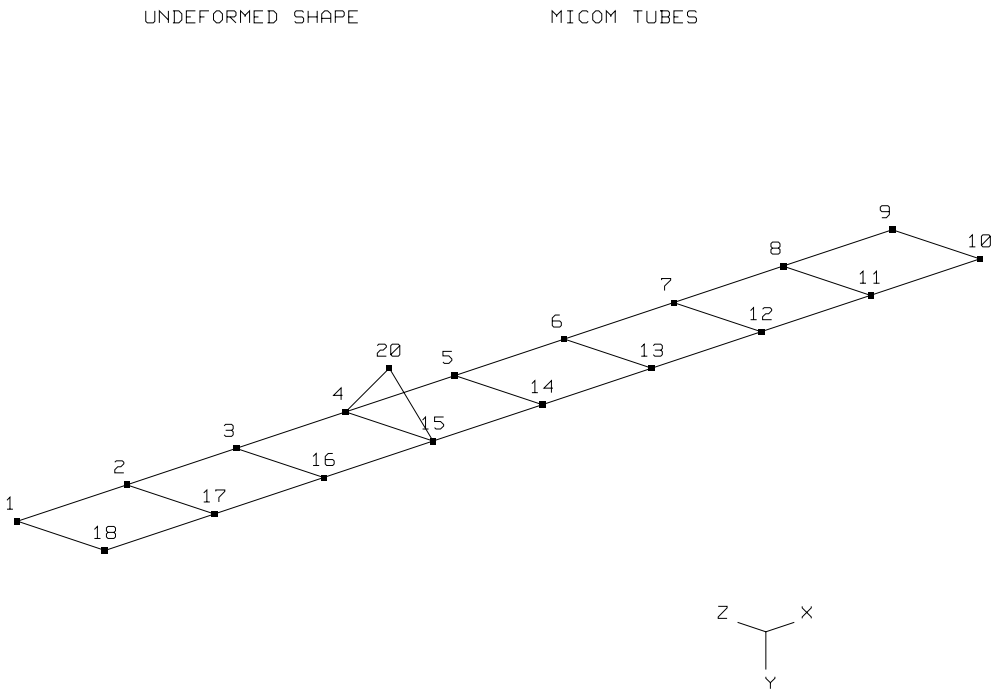

(a) Test Location Numbers

Location:	1	2	3	4	5	6	7	8	9	10	11	12	13	14	15	16	17	18	20
X	x																		
Y																			x
Z															x		x		

(b) Excitation Positions (4)

Location:	1	2	3	4	5	6	7	8	9	10	11	12	13	14	15	16	17	18	20
X	x								x	x									
Y	x								x	x									x
Z	x	x	x	x	x	x	x	x	x	x	x	x	x	x	x	x	x	x	

(c) Accelerometer Positions (25)

Fig. 3. Test Set-Up

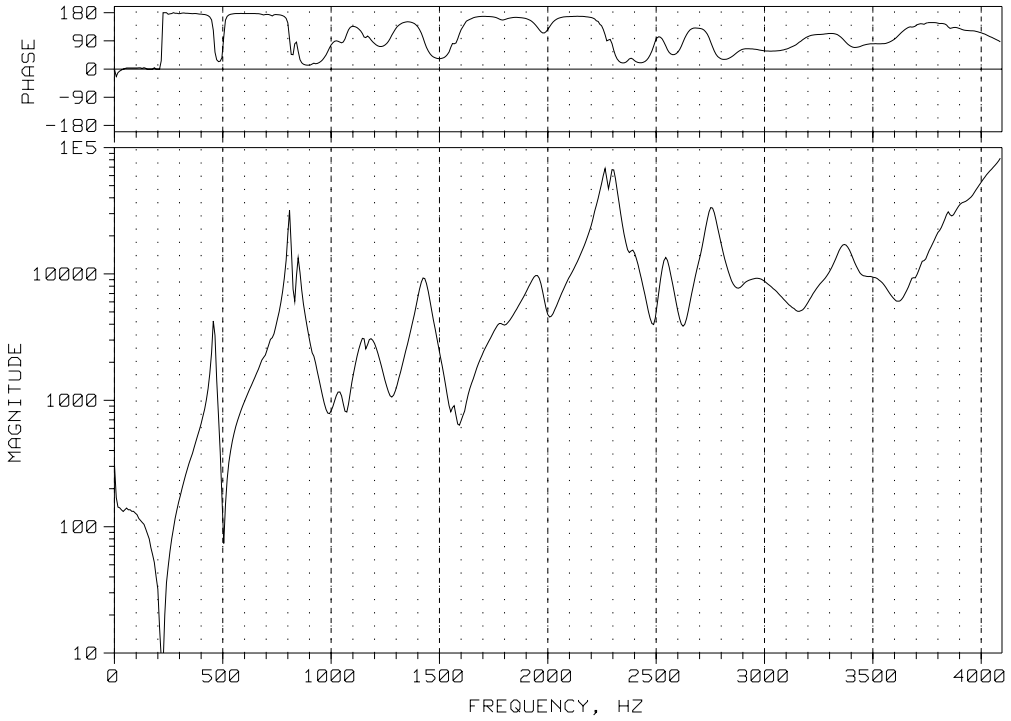

Fig. 4a. Driving-Point FRF for Tube 1 at Position 15Z

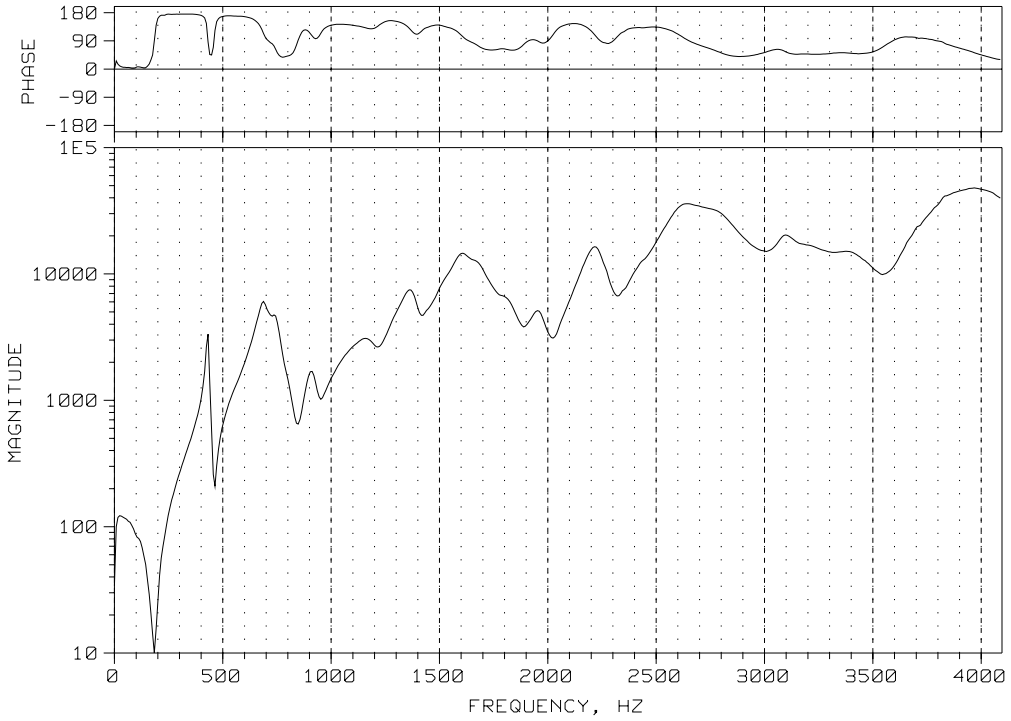

Fig. 4b. Driving-Point FRF for Tube 2 at Position 15Z

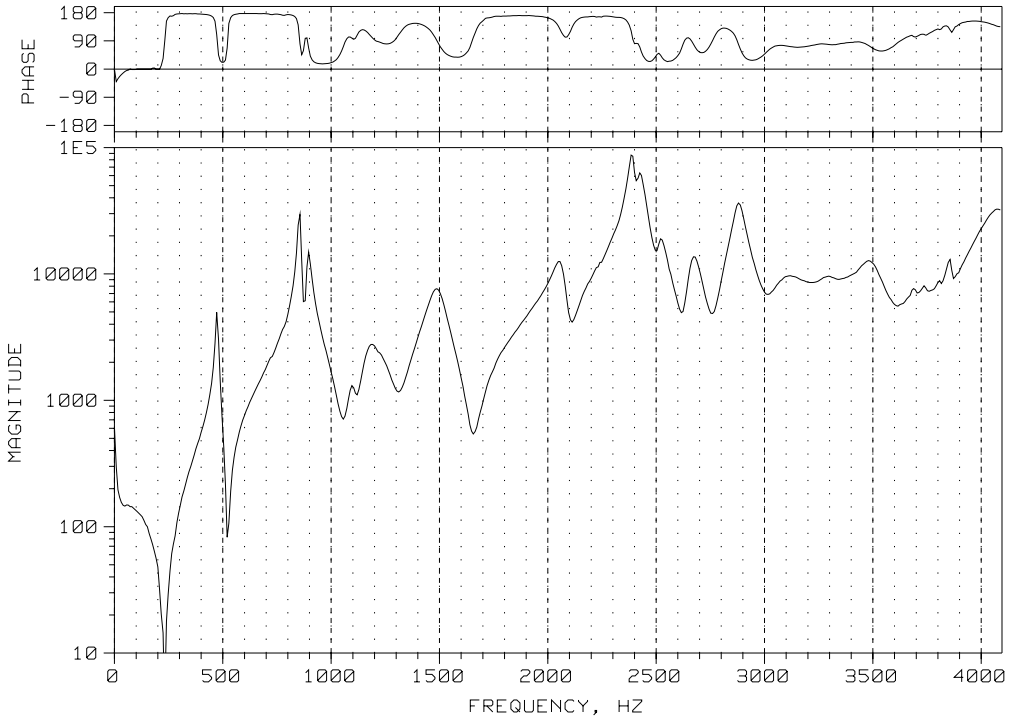

Fig. 4c. Driving-Point FRF for Tube 3 at Position 15Z

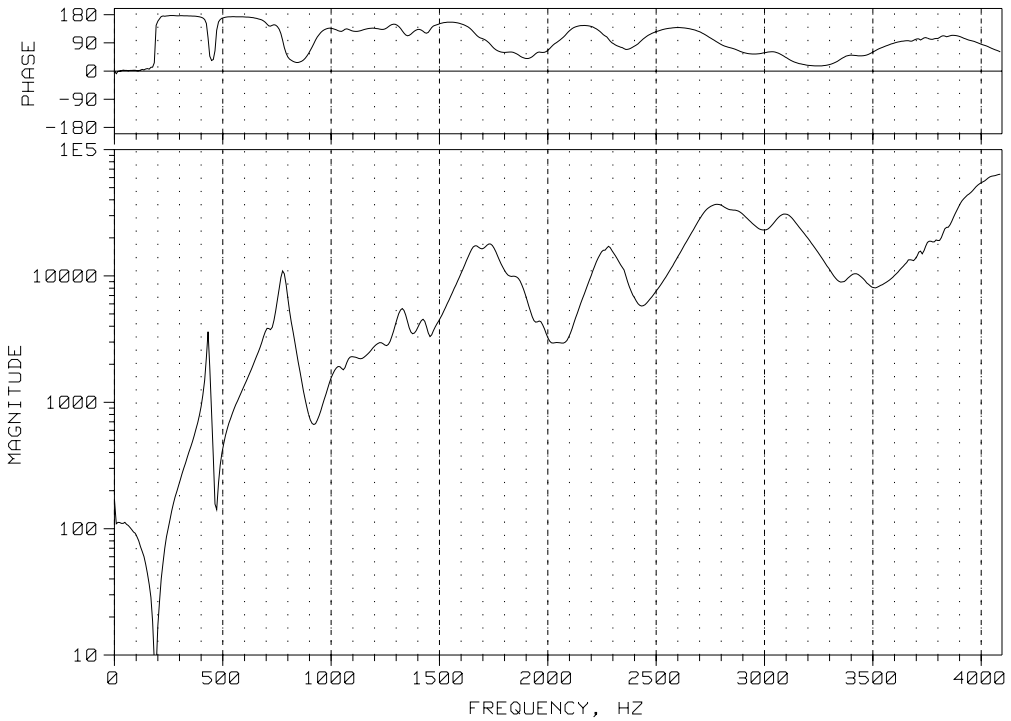

Fig. 4d. Driving-Point FRF for Tube 4 at Position 15Z

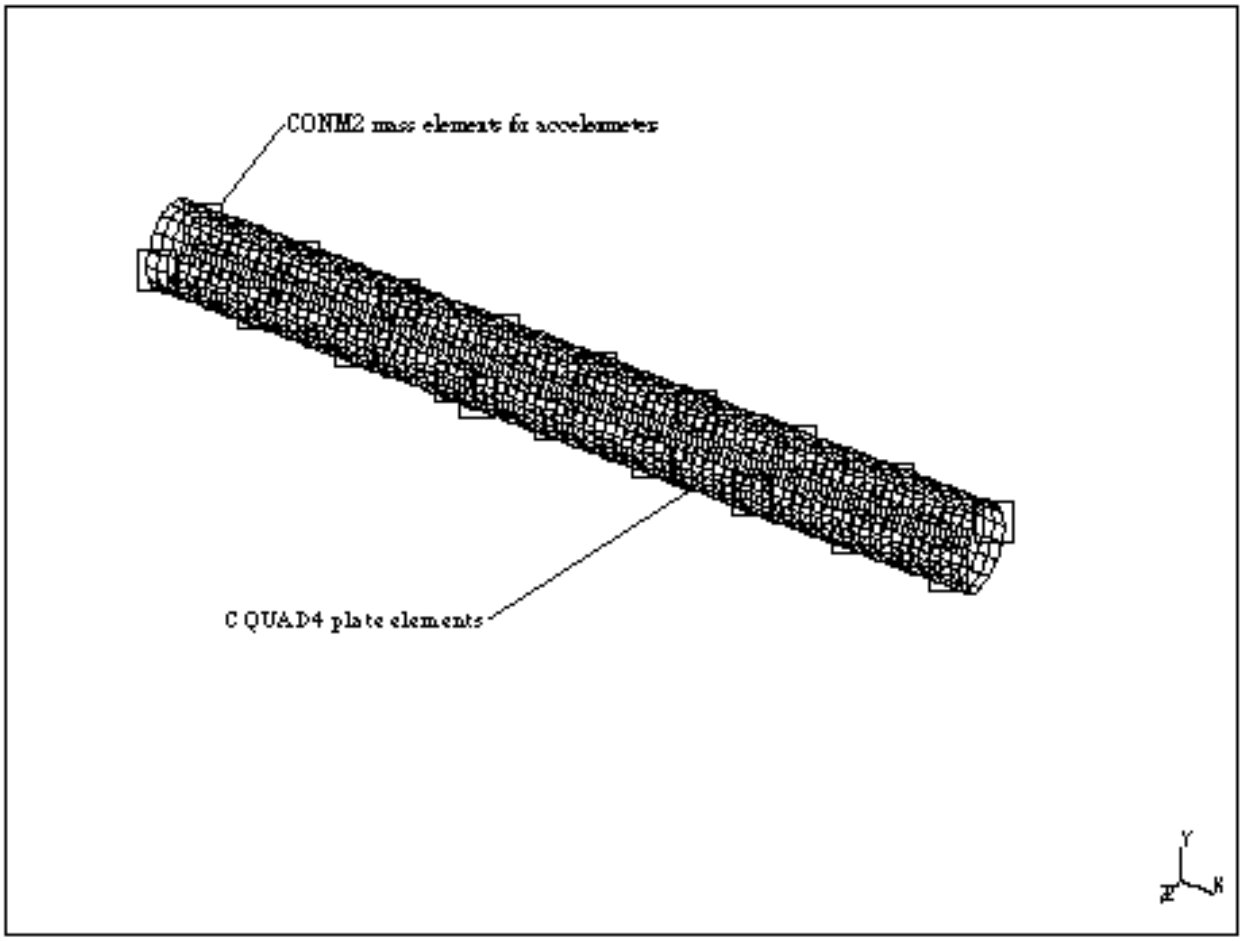

Figure 5. Finite Element Model

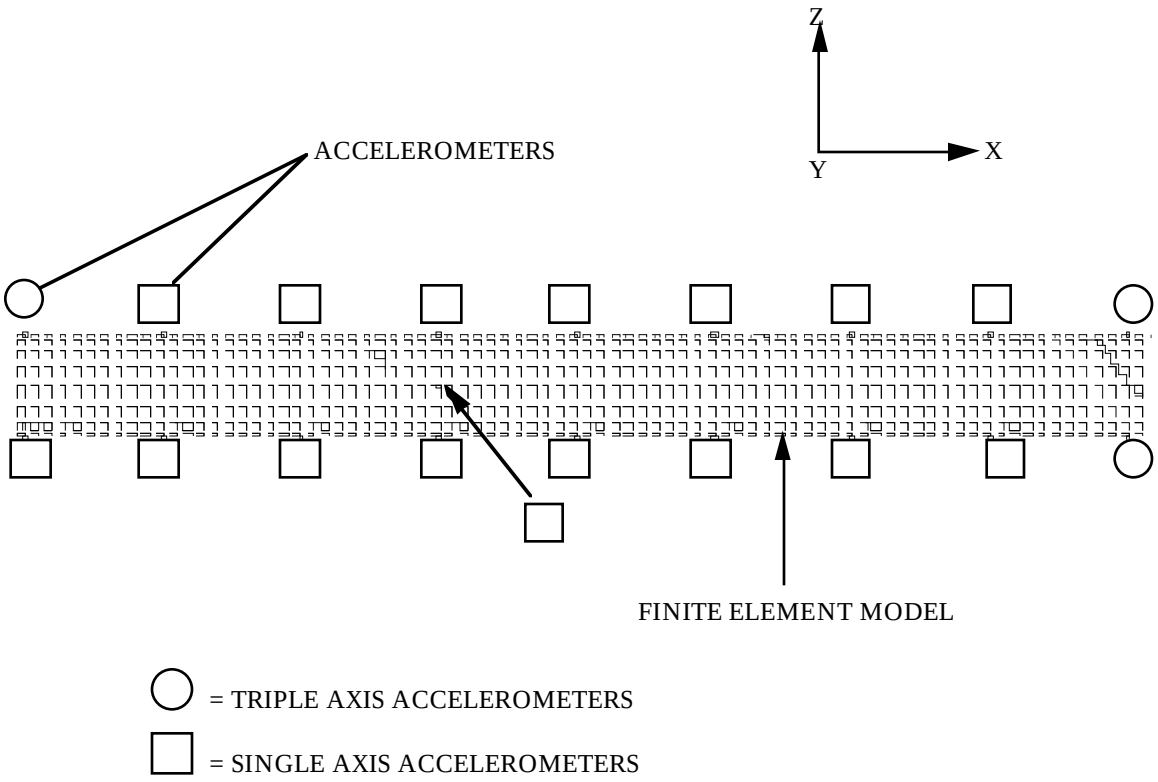

Figure 6. Accelerometer locations and coordinate system.

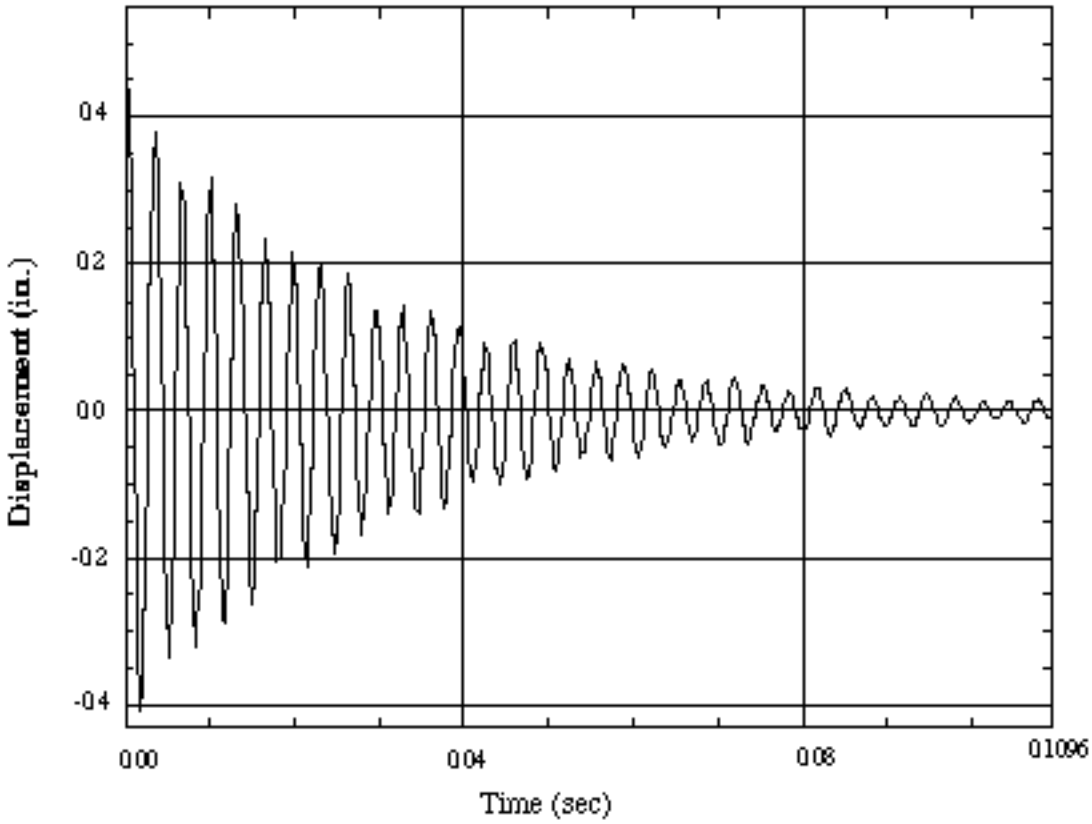

Figure 7a. Transient Response for node 10374 in y-direction. First bending mode decay

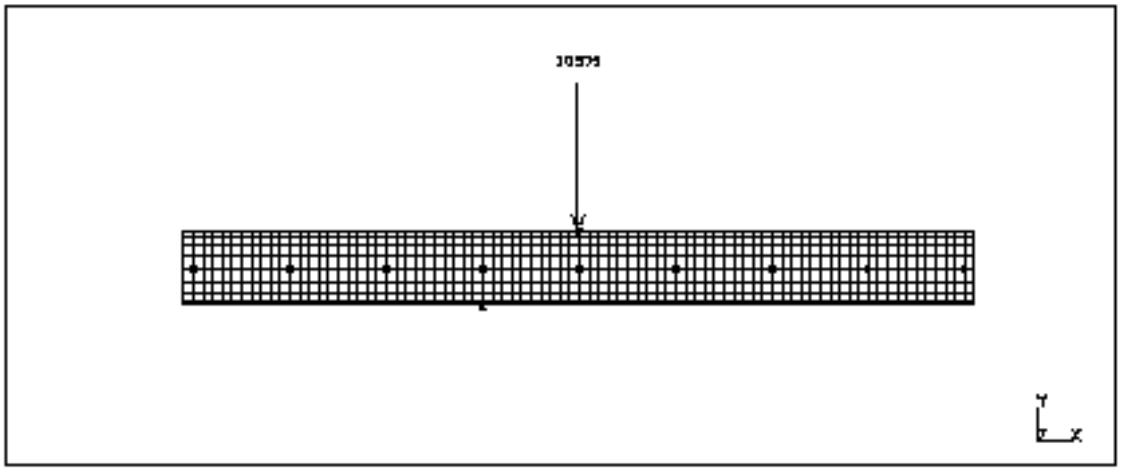

Figure 7b. Location of the node 10374 on the Finite Element model

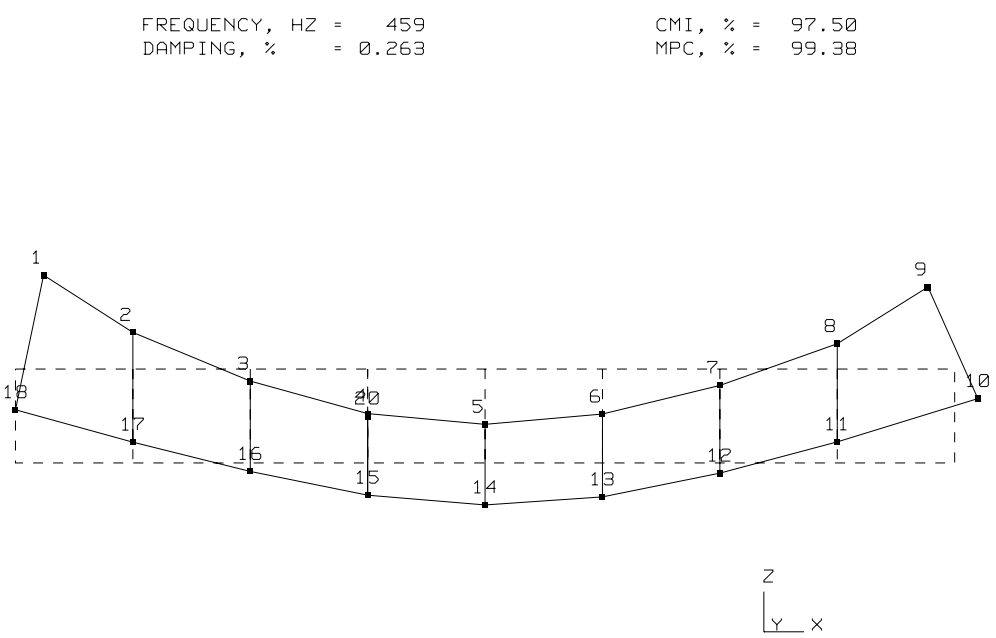

Fig. 8a. 1st Bending Mode of Tube 1 (Mode 1B-Z)

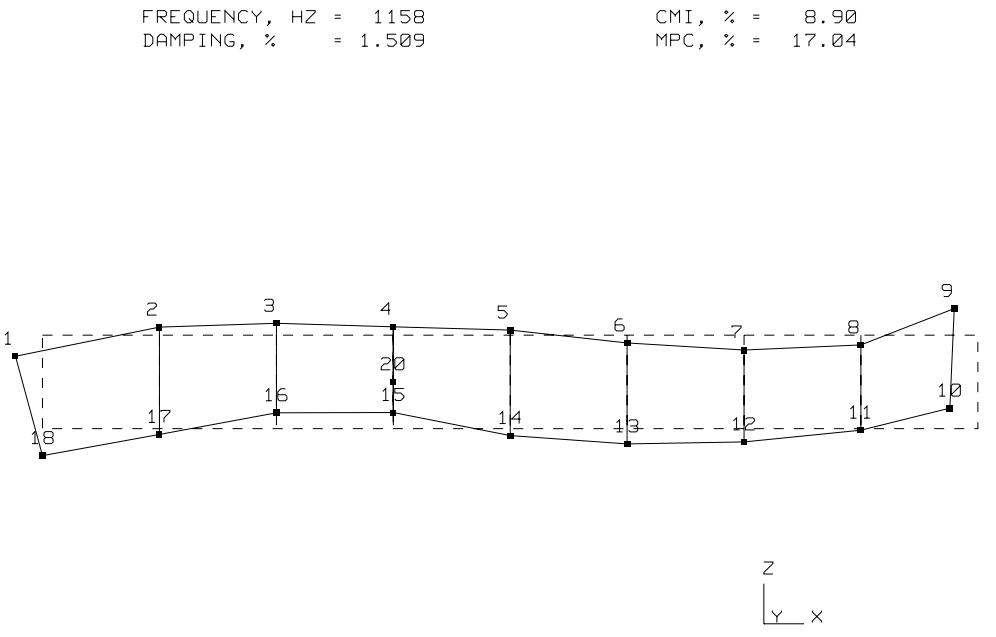

Fig. 8b. 2nd Bending Mode of Tube 1 (Mode 2B-Z)

FREQUENCY, HZ = 2195 CMI, % = 92.94
DAMPING, % = 0.632 MPC, % = 98.70

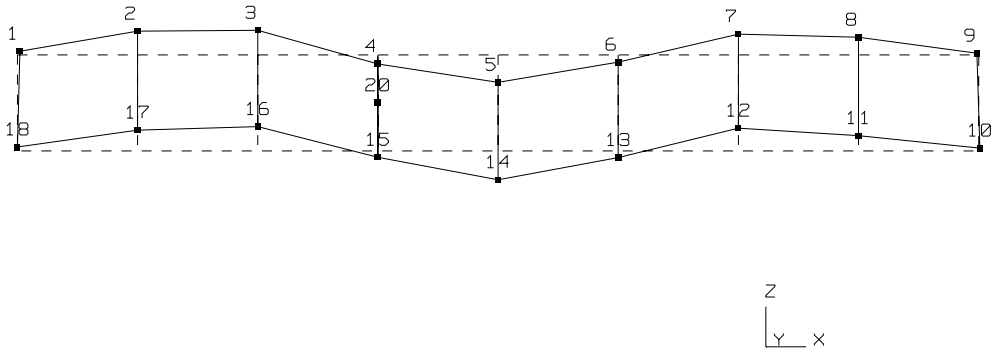

Fig. 8c. 3rd Bending Mode of Tube 1 (Mode 3B-Z)

FREQUENCY, HZ = 2298 CMI, % = 89.30
DAMPING, % = 0.574 MPC, % = 96.87

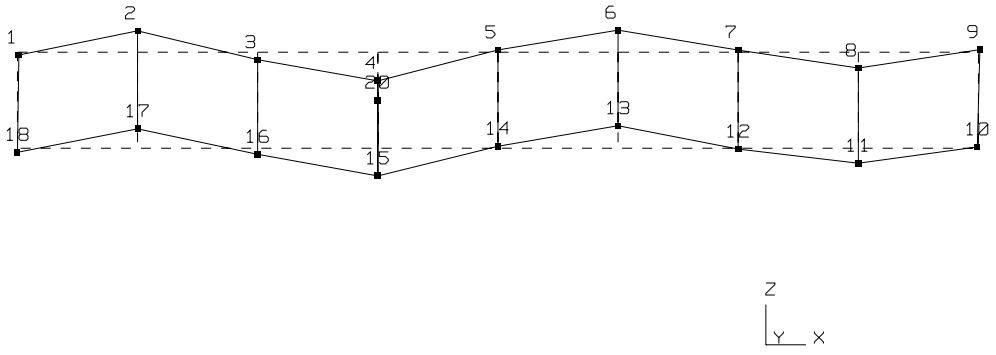

Fig. 8d. 4th Bending Mode of Tube 1 (Mode 4B-Z)

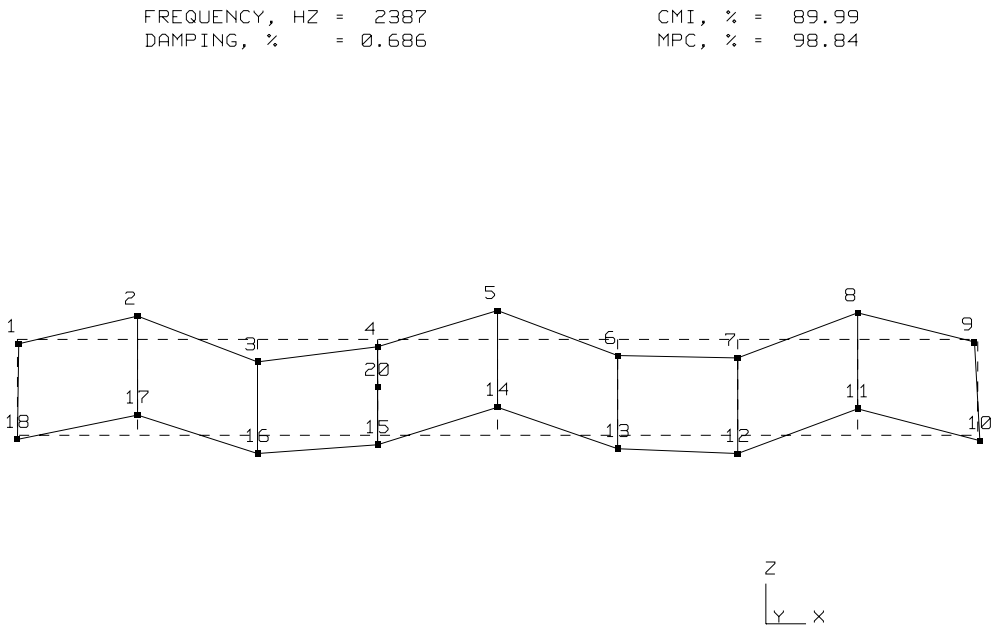

Fig. 8e. 5th Bending Mode of Tube 1 (Mode 5B-Z)

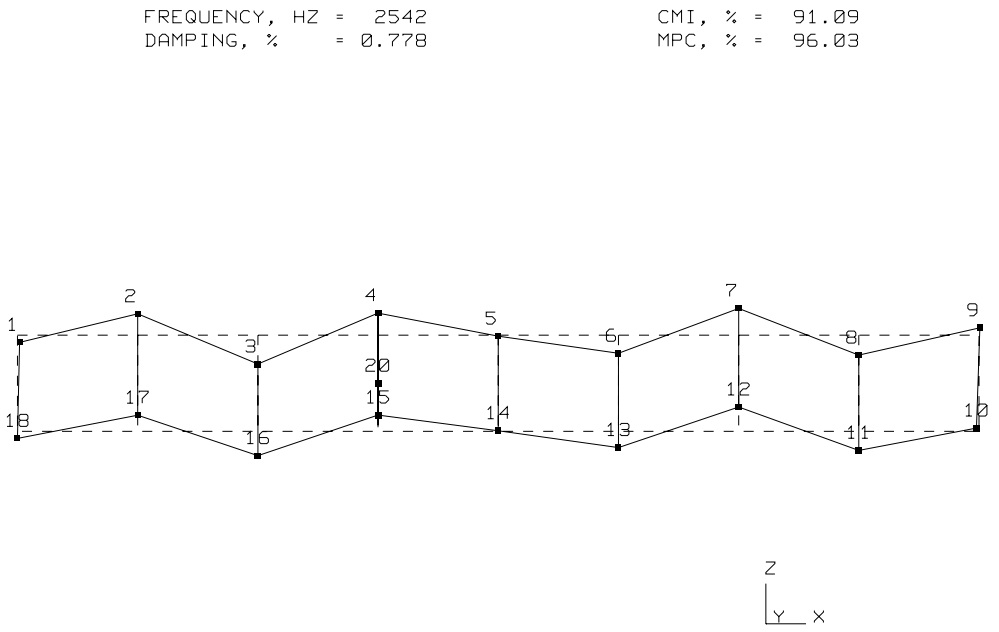

Fig. 8f. 6th Bending Mode of Tube 1 (Mode 6B-Z)

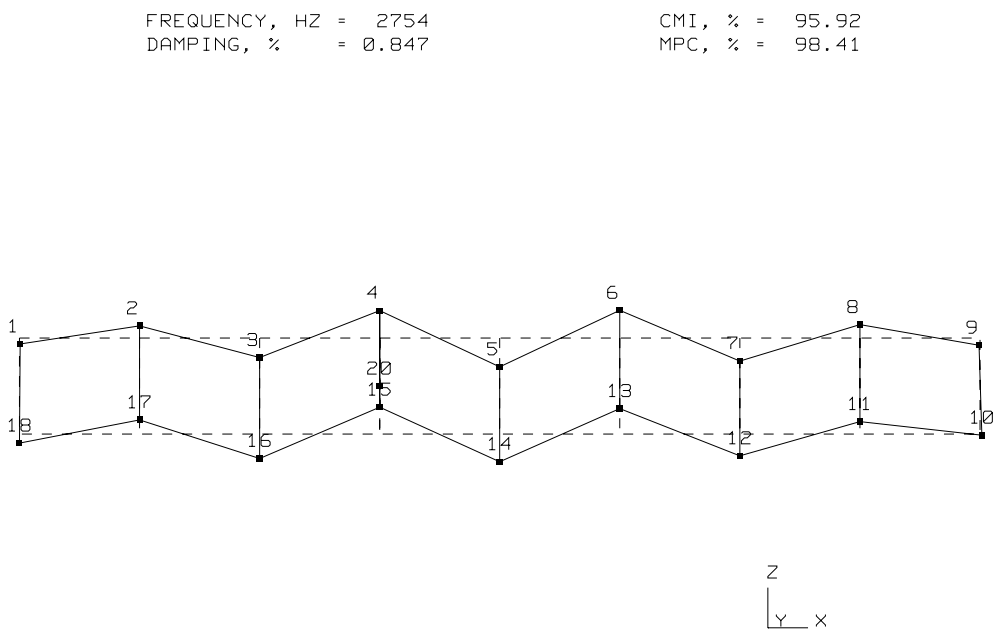

Fig. 8g. 7th Bending Mode of Tube 1 (Mode 7B-Z)

FREQUENCY, HZ = 688 CMI, % = 93.71
DAMPING, % = 0.548 MPC, % = 98.78

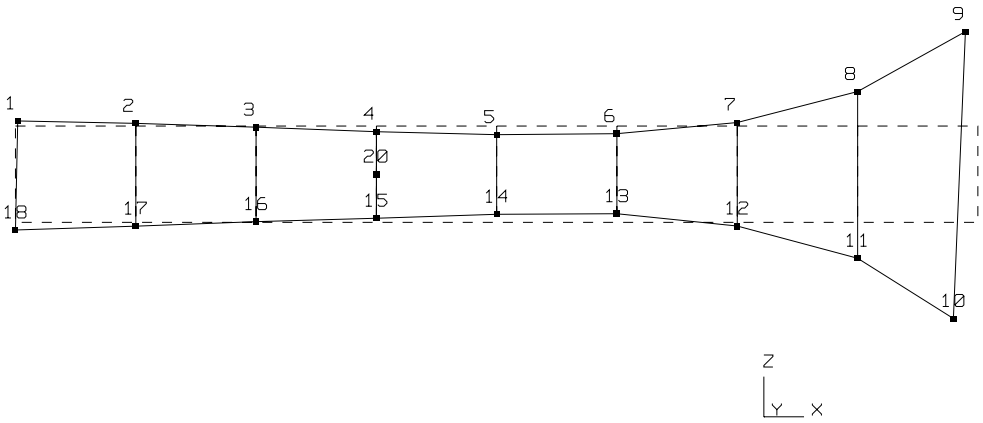

Fig. 8h. Rightside Love Mode of Tube 1 (Mode R-Love)

FREQUENCY, HZ = 726 CMI, % = 97.08
DAMPING, % = 0.524 MPC, % = 99.18

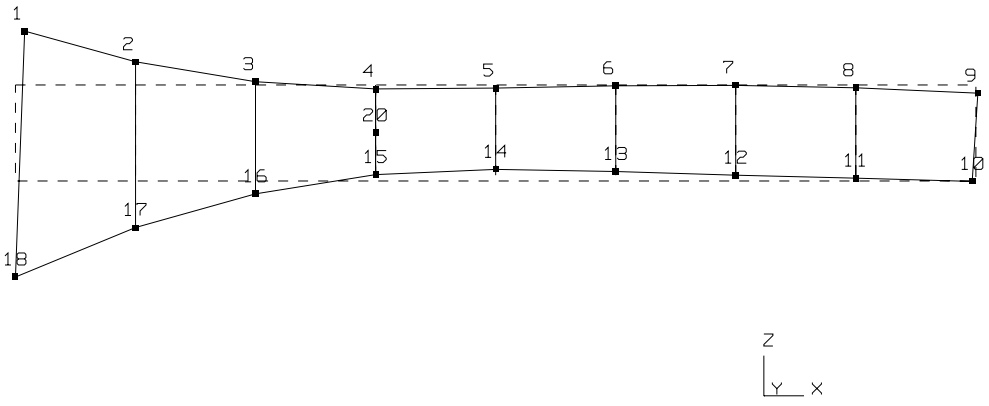

Fig. 8i. Leftside Love Mode of Tube 1 (Mode L-Love)

FREQUENCY, HZ = 808 CMI, % = 98.09
DAMPING, % = 0.200 MPC, % = 99.37

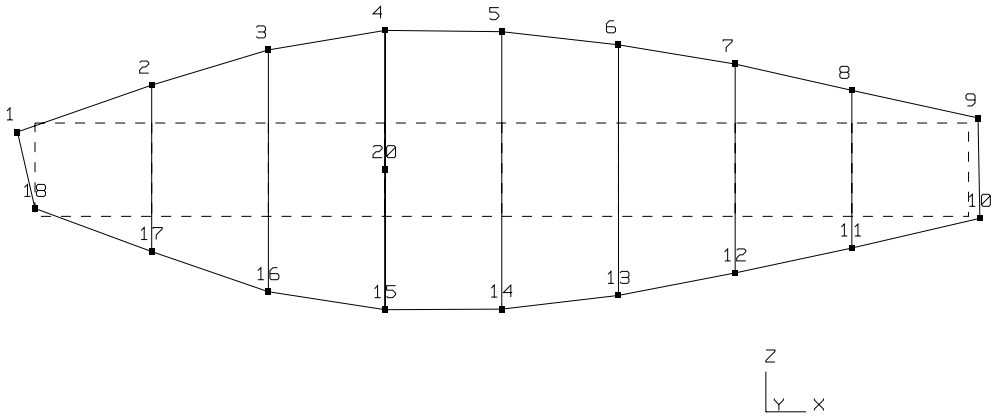

Fig. 8j. 1st Breathing Mode of Tube 1 (Mode 1BR)

FREQUENCY, HZ = 845 CMI, % = 94.58
DAMPING, % = 0.459 MPC, % = 97.93

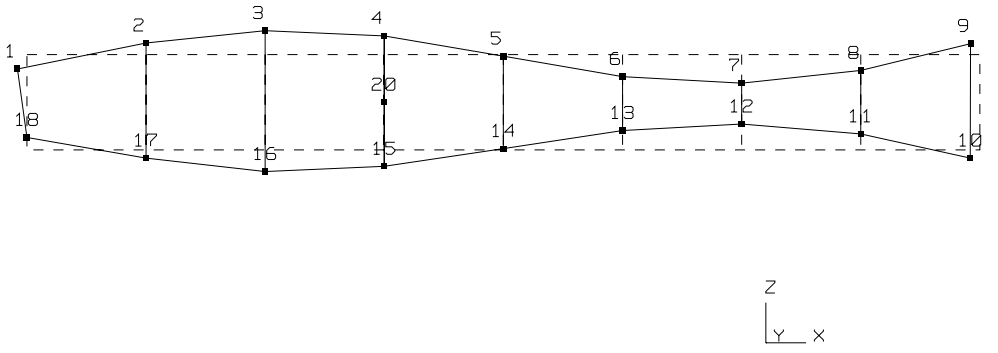

Fig. 8k. 2nd Breathing Mode of Tube 1 (Mode 2BR)

FREQUENCY, HZ = 1045 CMI, % = 7.79
DAMPING, % = 2.529 MPC, % = 25.17

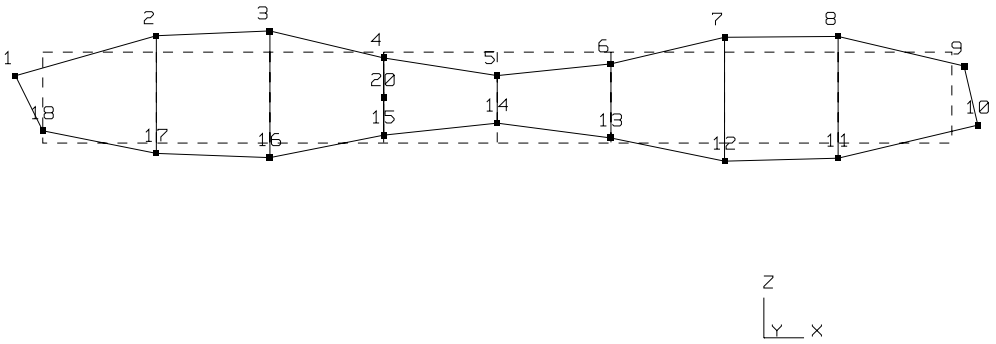

Fig. 8l. 3rd Breathing Mode of Tube 1 (Mode 3BR)

FREQUENCY, HZ = 1430 CMI, % = 63.86
DAMPING, % = 1.844 MPC, % = 70.12

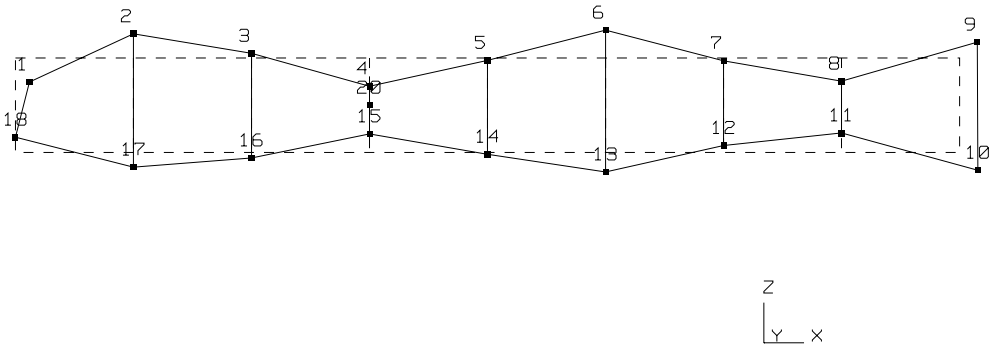

Fig. 8m. 4th Breathing Mode of Tube 1 (Mode 4BR)

FREQUENCY, HZ = 1964 CMI, % = 89.08
DAMPING, % = 1.598 MPC, % = 98.72

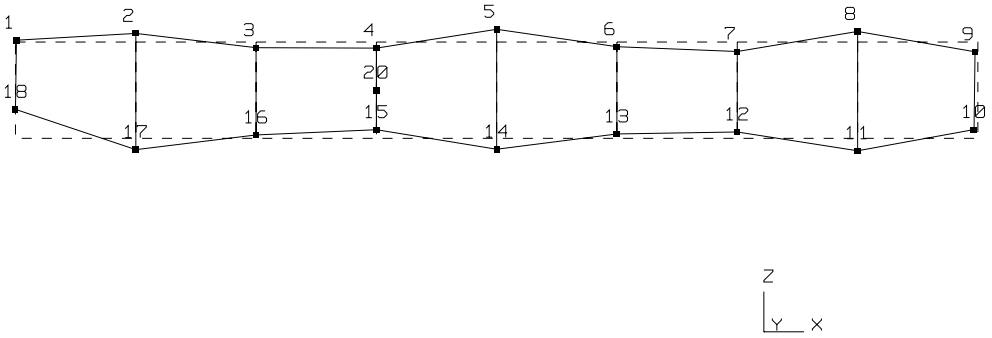

Fig. 8n. 5th Breathing Mode of Tube 1 (Mode 5BR)

FREQUENCY, HZ = 2489 CMI, % = 31.89
DAMPING, % = 1.219 MPC, % = 65.26

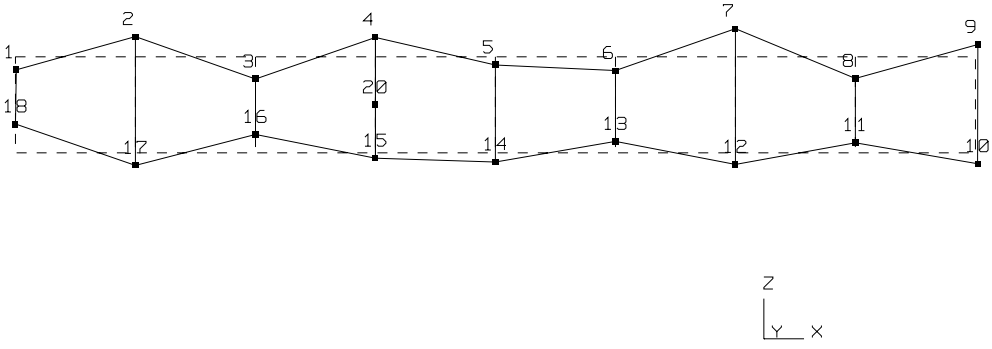

Fig. 8o. 6th Breathing Mode of Tube 1 (Mode 6BR)

FREQUENCY, HZ = 431 CMI, % = 98.26
DAMPING, % = 0.320 MPC, % = 99.81

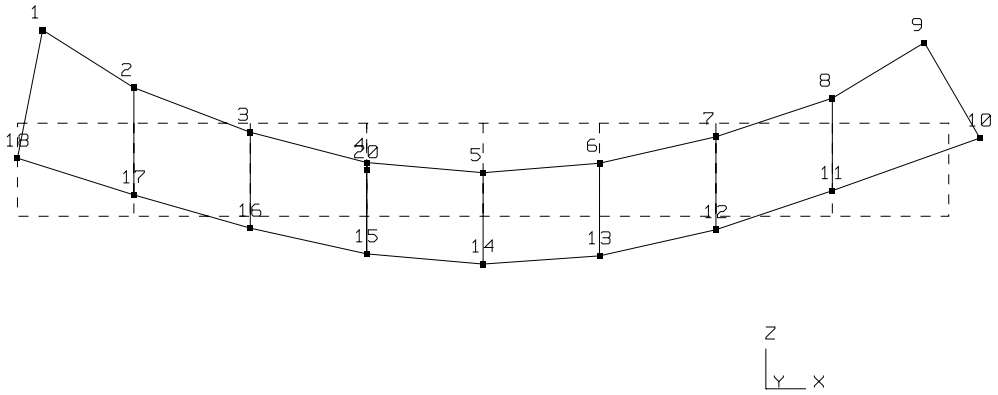

Fig. 9a. 1st Bending Mode of Tube 2 (Mode 1B-Z)

FREQUENCY, HZ = 1184 CMI, % = 5.03
DAMPING, % = 5.078 MPC, % = 32.05

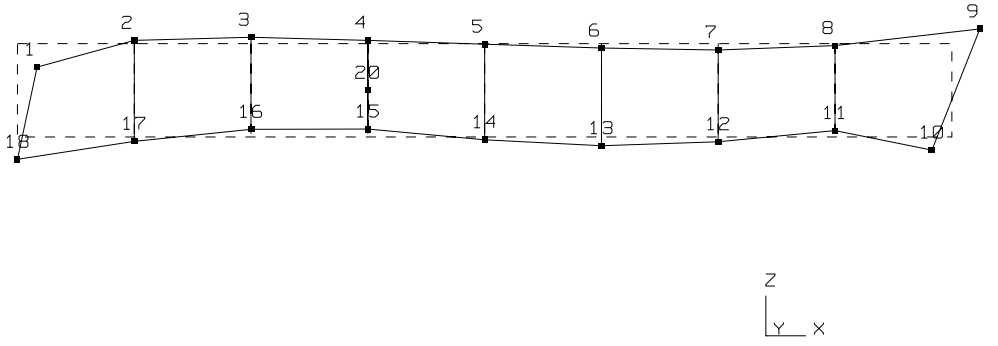

Fig. 9b. 2nd Bending Mode of Tube 2 (Mode 2B-Z)

FREQUENCY, HZ = 1606 CMI, % = 48.75
DAMPING, % = 3.018 MPC, % = 88.33

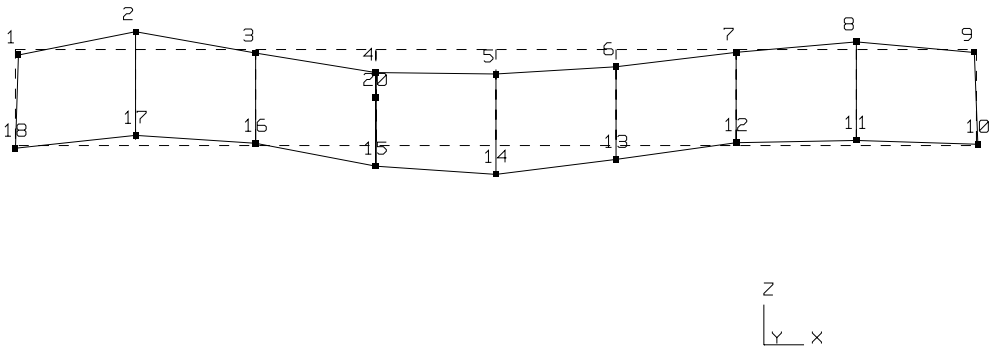

Fig. 9c. 3rd Bending Mode of Tube 2 (Mode 3B-Z)

FREQUENCY, HZ = 1674 CMI, % = 74.01
DAMPING, % = 2.825 MPC, % = 90.22

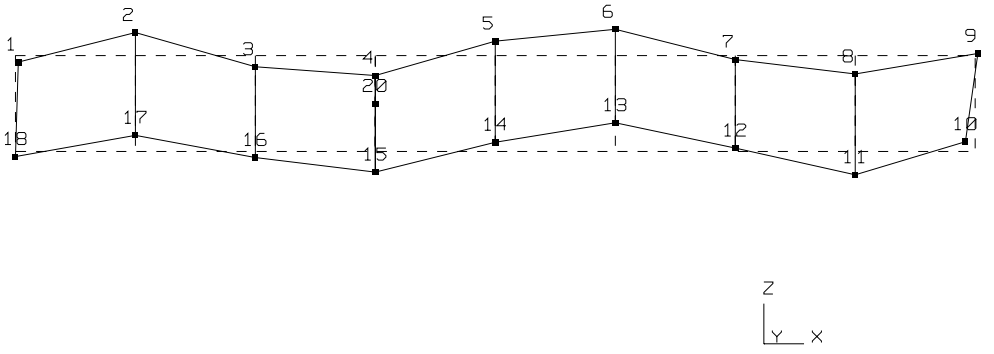

Fig. 9d. 4th Bending Mode of Tube 2 (Mode 4B-Z)

FREQUENCY, HZ = 1801 CMI, % = 59.56
DAMPING, % = 2.766 MPC, % = 85.67

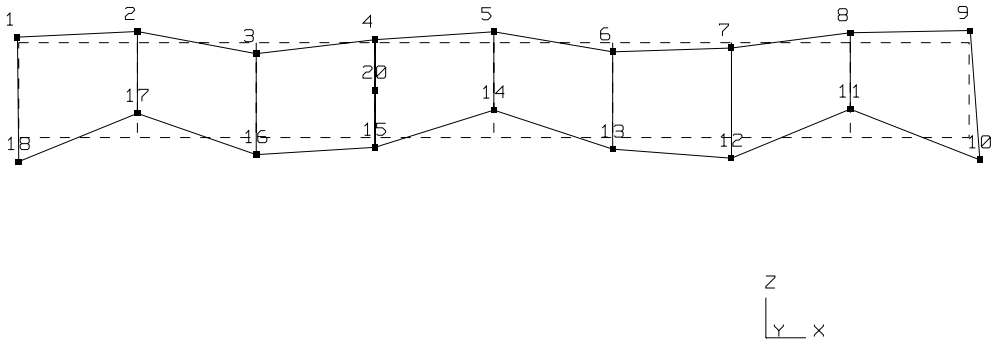

Fig. 9e. 5th Bending Mode of Tube 2 (Mode 5B-Z)

FREQUENCY, HZ = 1958 CMI, % = 50.35
DAMPING, % = 2.139 MPC, % = 95.48

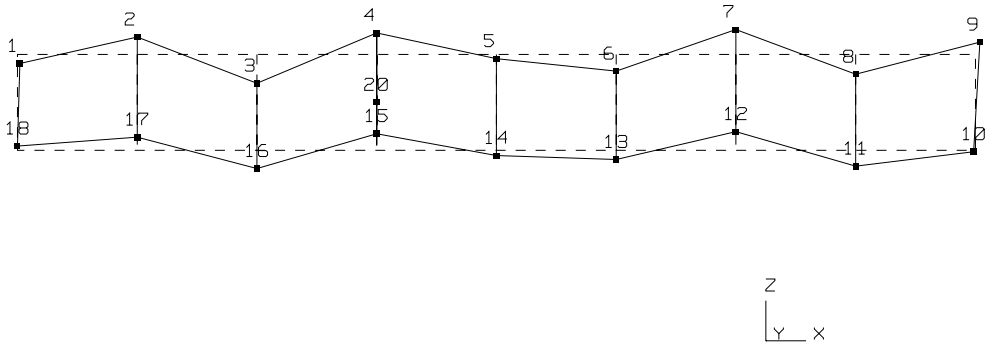

Fig. 9f. 6th Bending Mode of Tube 2 (Mode 6B-Z)

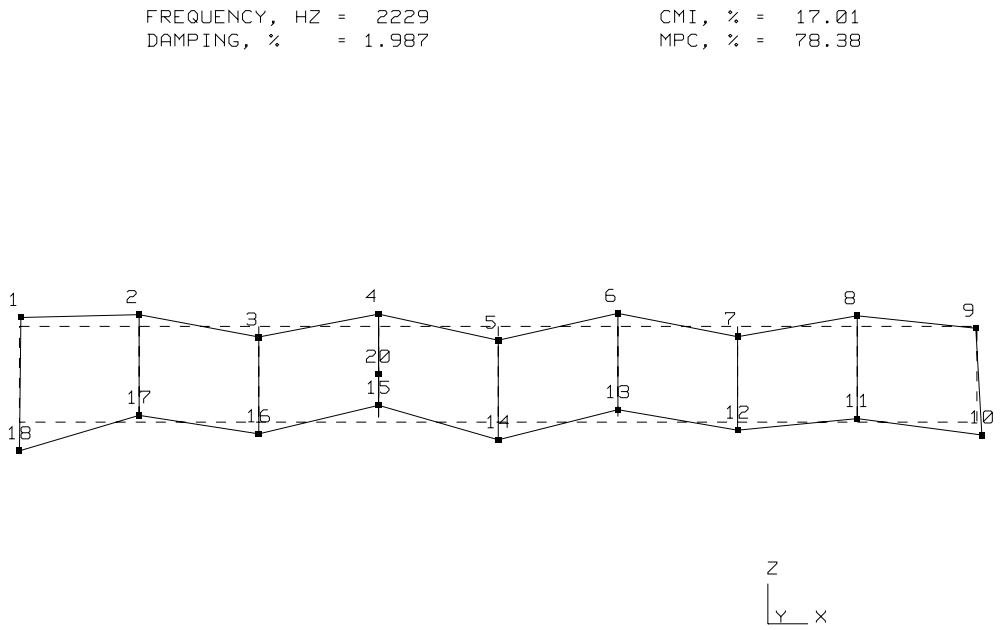

Fig. 9g. 7th Bending Mode of Tube 2 (Mode 7B-Z)

FREQUENCY, HZ = 555 CMI, % = 67.20
DAMPING, % = 2.786 MPC, % = 84.13

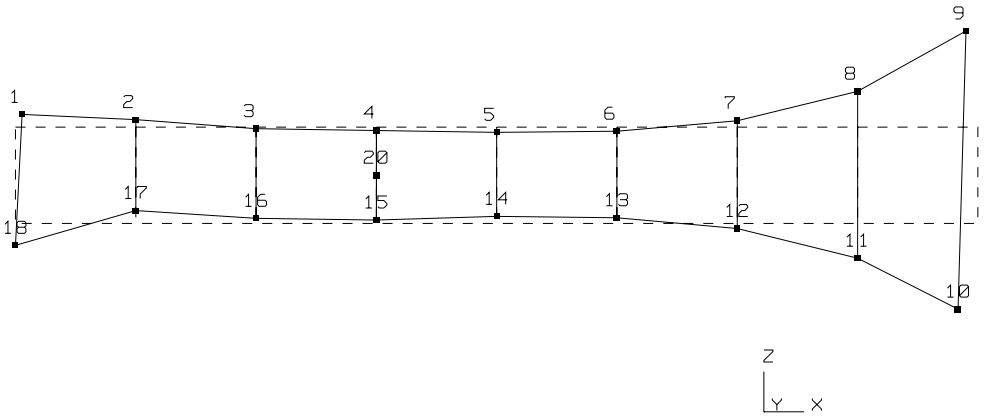

Fig. 9h. Rightside Love Mode of Tube 2 (Mode R-Love)

FREQUENCY, HZ = 575 CMI, % = 88.16
DAMPING, % = 2.731 MPC, % = 92.60

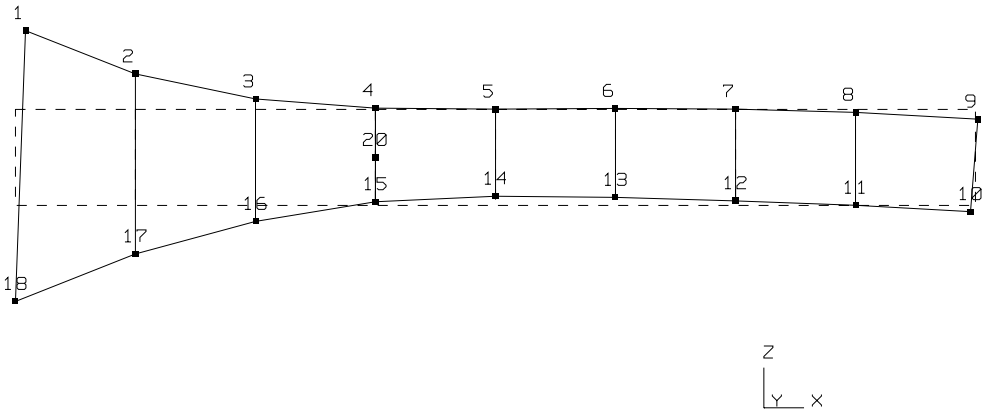

Fig. 9i. Leftside Love Mode of Tube 2 (Mode L-Love)

FREQUENCY, HZ = 691 CMI, % = 88.87
DAMPING, % = 3.280 MPC, % = 98.26

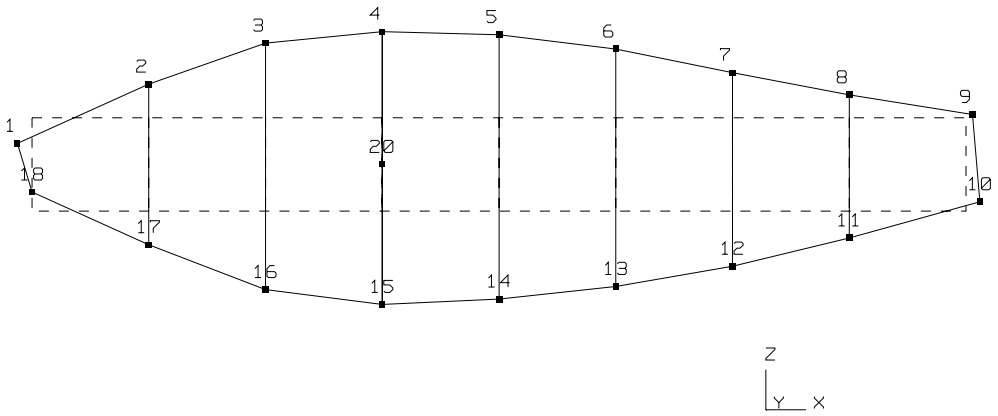

Fig. 9j. 1st Breathing Mode of Tube 2 (Mode 1BR)

FREQUENCY, HZ = 741 CMI, % = 93.53
DAMPING, % = 2.270 MPC, % = 98.93

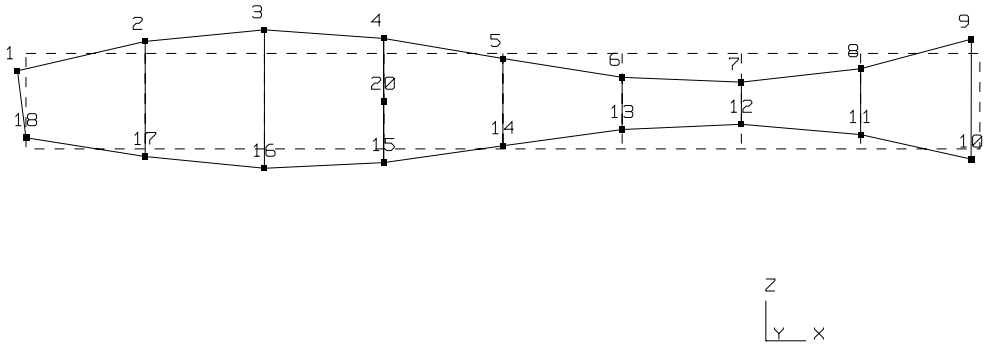

Fig. 9k. 2nd Breathing Mode of Tube 2 (Mode 2BR)

FREQUENCY, HZ = 911 CMI, % = 46.76
DAMPING, % = 3.136 MPC, % = 61.13

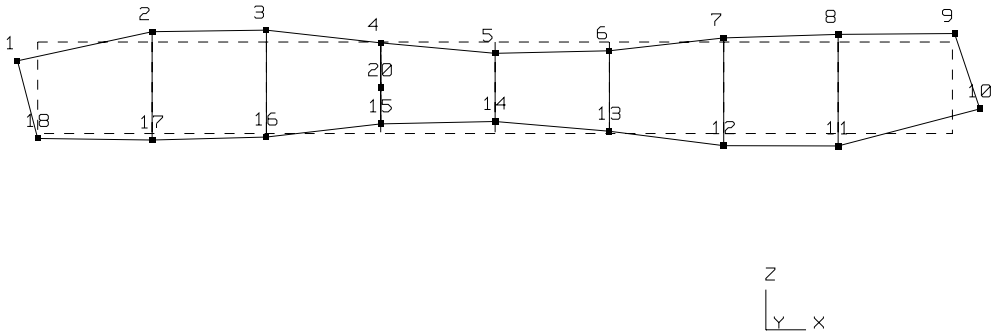

Fig. 9l. 3rd Breathing Mode of Tube 2 (Mode 3BR)

FREQUENCY, HZ = 1377 CMI, % = 72.41
DAMPING, % = 2.654 MPC, % = 85.74

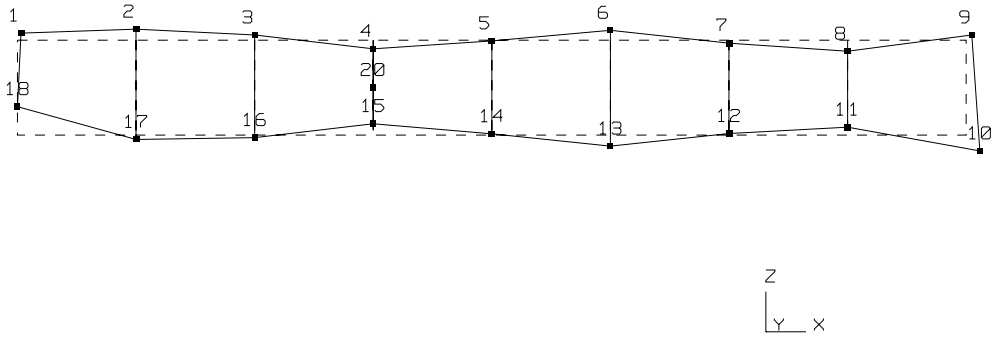

Fig. 9m. 4th Breathing Mode of Tube 2 (Mode 4BR)

FREQUENCY, HZ = 1745 CMI, % = 27.56
DAMPING, % = 2.858 MPC, % = 71.56

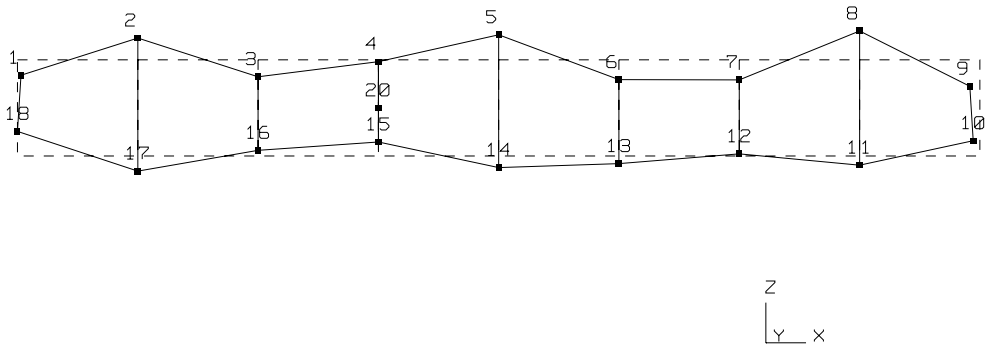

Fig. 9n. 5th Breathing Mode of Tube 2 (Mode 5BR)

FREQUENCY, HZ = 2434 CMI, % = 80.29
DAMPING, % = 1.727 MPC, % = 93.67

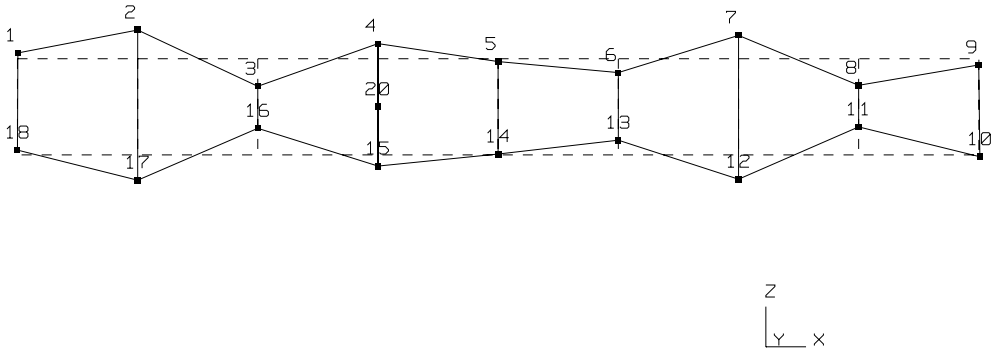

Fig. 9o. 6th Breathing Mode of Tube 2 (Mode 6BR)

FREQUENCY, HZ = 474 CMI, % = 97.74
DAMPING, % = 0.260 MPC, % = 98.90

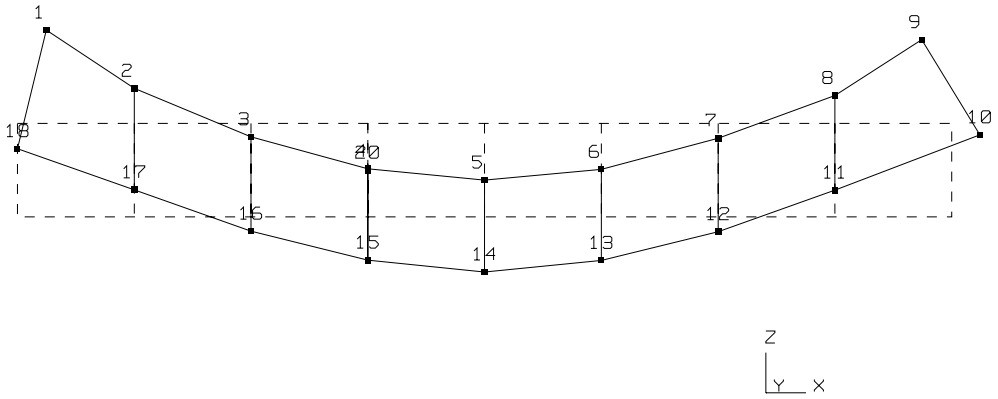

Fig. 10a. 1st Bending Mode of Tube 3 (Mode 1B-Z)

FREQUENCY, HZ = 1178 CMI, % = 22.76
DAMPING, % = 3.151 MPC, % = 39.42

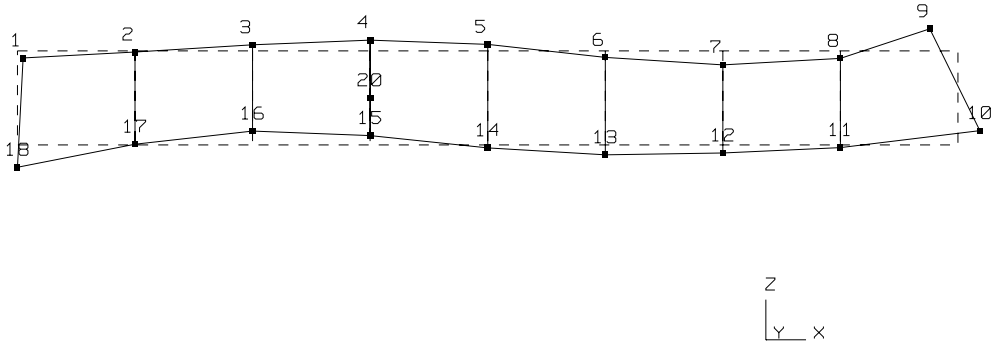

Fig. 10b. 2nd Bending Mode of Tube 3 (Mode 2B-Z)

FREQUENCY, HZ = 2305 CMI, % = 70.01
DAMPING, % = 0.291 MPC, % = 92.09

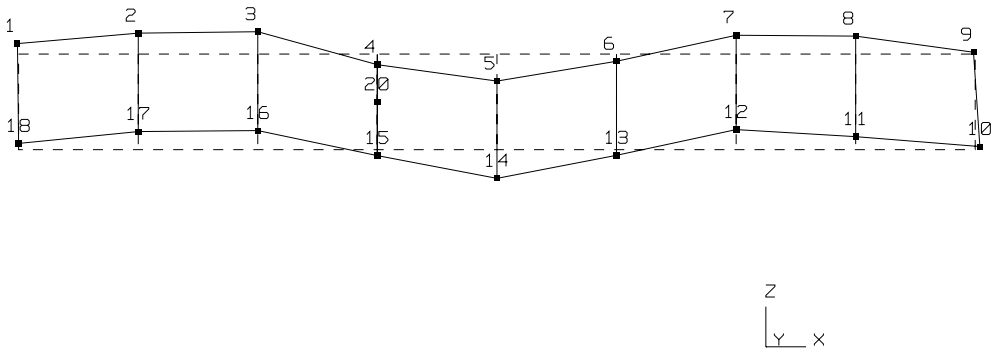

Fig. 10c. 3rd Bending Mode of Tube 3 (Mode 3B-Z)

FREQUENCY, HZ = 2424 CMI, % = 88.48
DAMPING, % = 0.597 MPC, % = 93.38

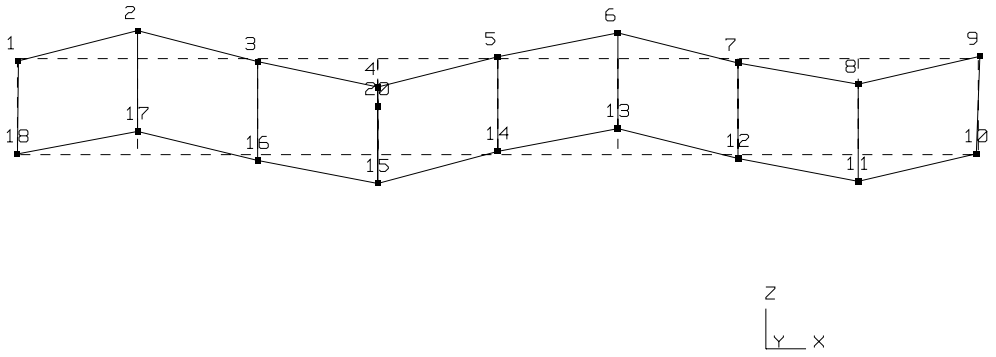

Fig. 10d. 4th Bending Mode of Tube 3 (Mode 4B-Z)

FREQUENCY, HZ = 2517 CMI, % = 90.36
DAMPING, % = 0.629 MPC, % = 96.36

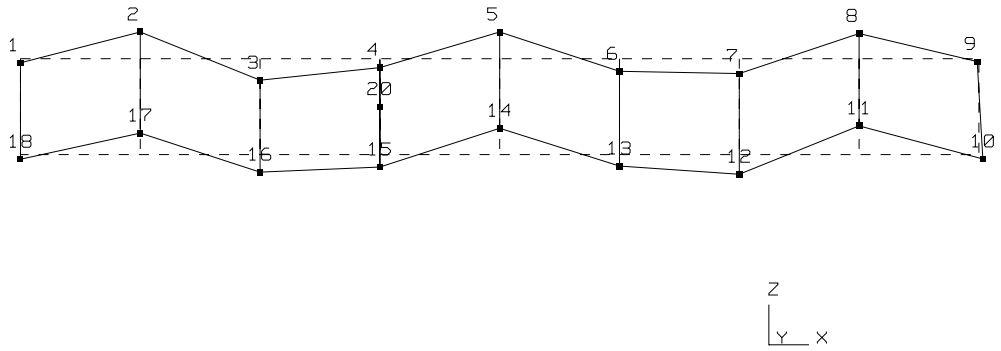

Fig. 10e. 5th Bending Mode of Tube 3 (Mode 5B-Z)

FREQUENCY, HZ = 2670 CMI, % = 84.29
DAMPING, % = 0.965 MPC, % = 91.57

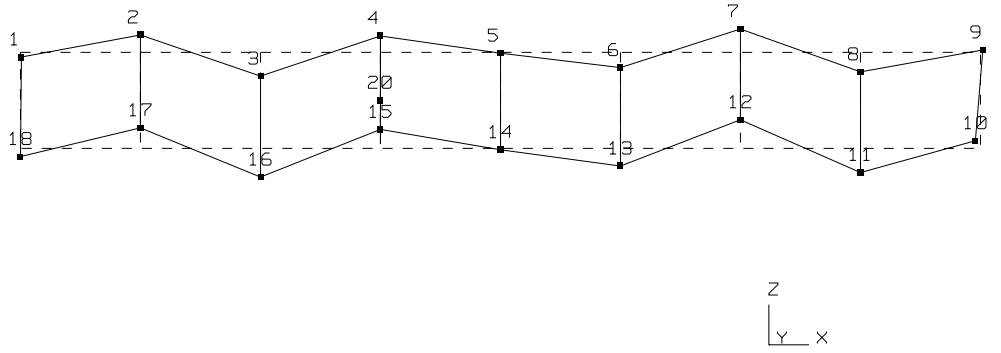

Fig. 10f. 6th Bending Mode of Tube 3 (Mode 6B-Z)

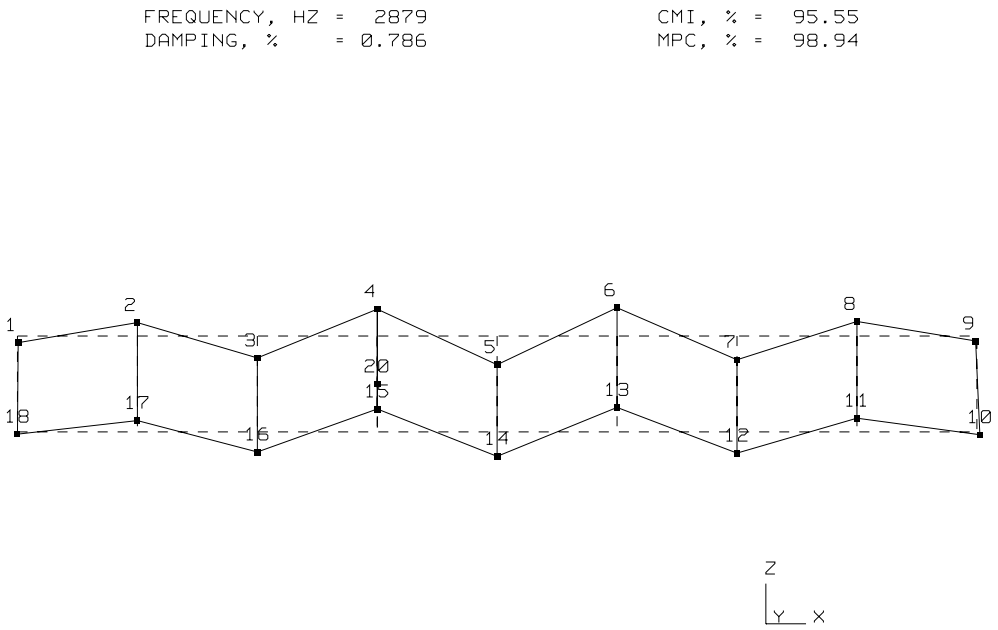

Fig. 10g. 7th Bending Mode of Tube 3 (Mode 7B-Z)

FREQUENCY, HZ = 724 CMI, % = 96.64
DAMPING, % = 0.489 MPC, % = 98.93

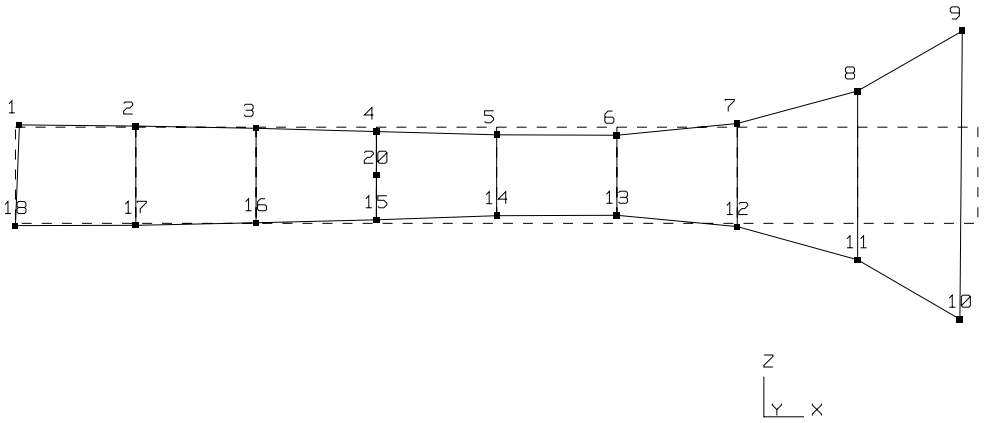

Fig. 10h. Rightside Love Mode of Tube 3 (Mode R-Love)

FREQUENCY, HZ = 784 CMI, % = 79.21
DAMPING, % = 1.019 MPC, % = 80.20

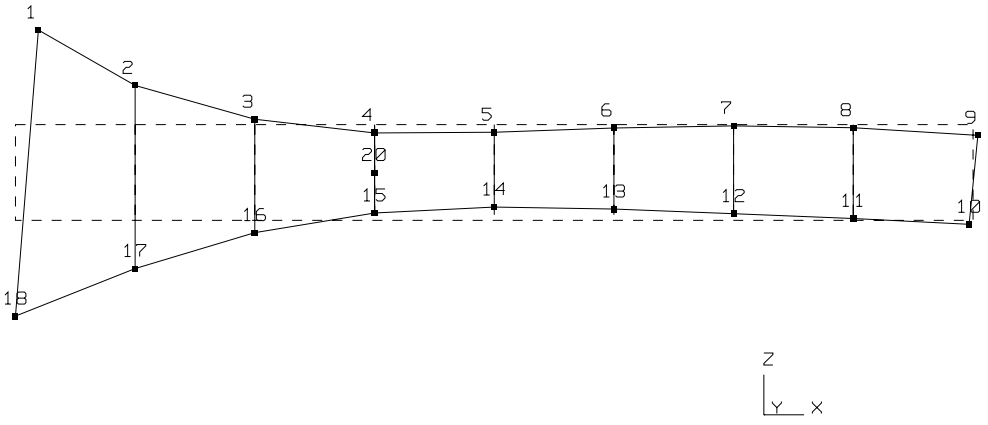

Fig. 10i. Leftside Love Mode of Tube 3 (Mode L-Love)

FREQUENCY, HZ = 854 CMI, % = 97.17
DAMPING, % = 0.182 MPC, % = 98.24

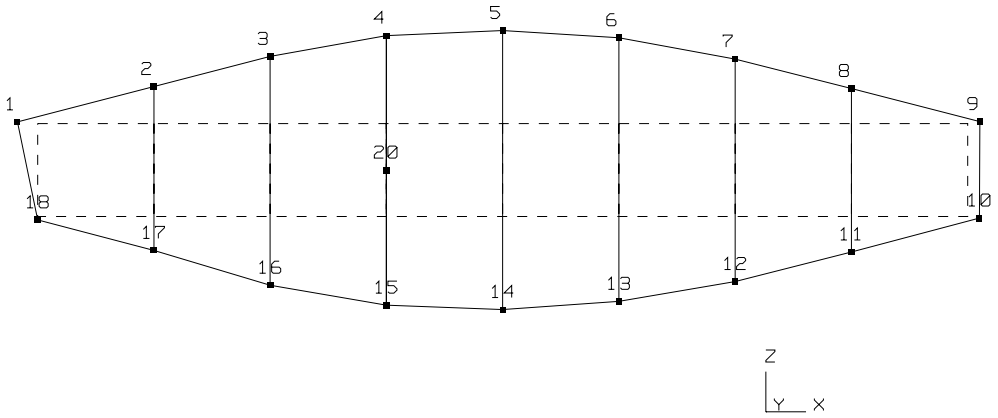

Fig. 10j. 1st Breathing Mode of Tube 3 (Mode 1BR)

FREQUENCY, HZ = 893 CMI, % = 83.45
DAMPING, % = 0.688 MPC, % = 86.37

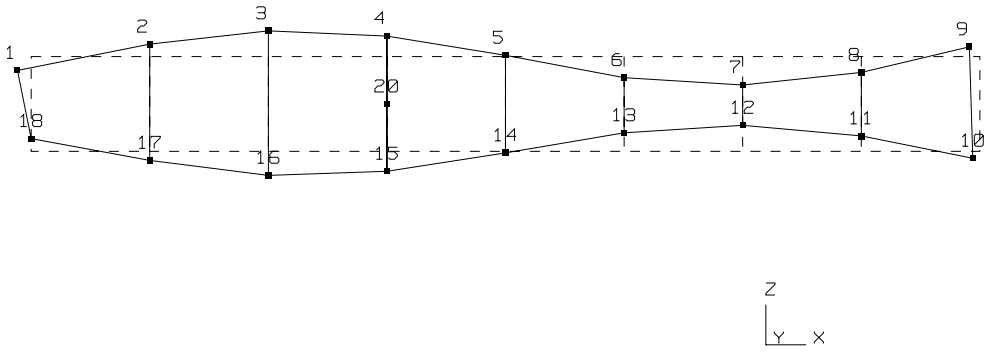

Fig. 10k. 2nd Breathing Mode of Tube 3 (Mode 2BR)

FREQUENCY, HZ = 1100 CMI, % = 73.97
DAMPING, % = 1.598 MPC, % = 76.79

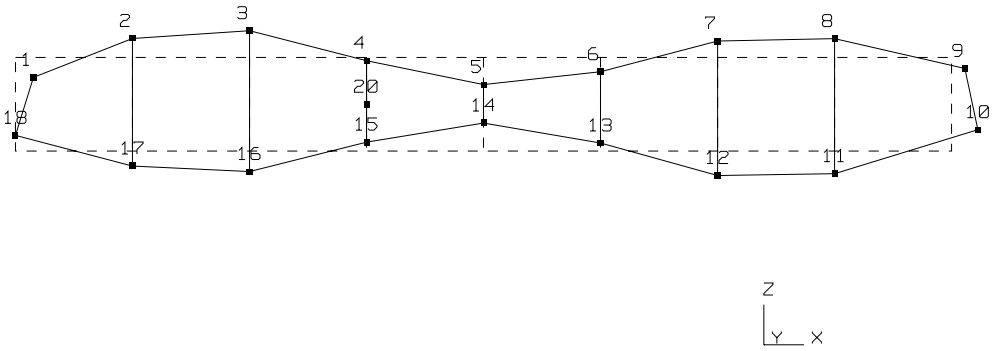

Fig. 10l. 3rd Breathing Mode of Tube 3 (Mode 3BR)

FREQUENCY, HZ = 1490 CMI, % = 35.06
DAMPING, % = 2.506 MPC, % = 37.62

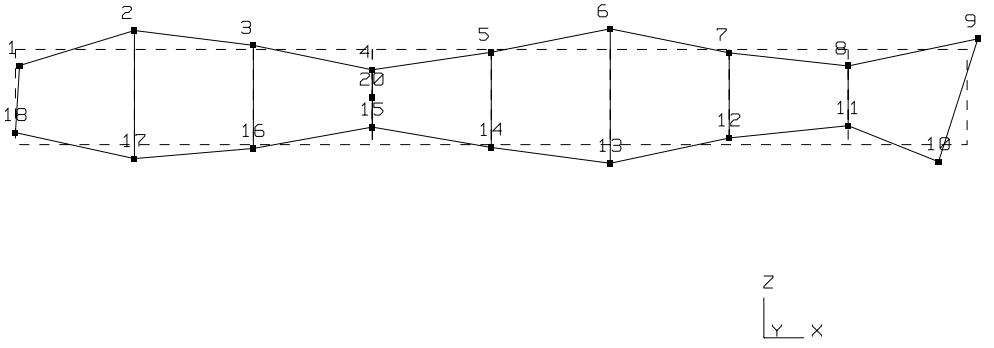

Fig. 10m. 4th Breathing Mode of Tube 3 (Mode 4BR)

FREQUENCY, HZ = 2064 CMI, % = 92.98
DAMPING, % = 1.185 MPC, % = 97.49

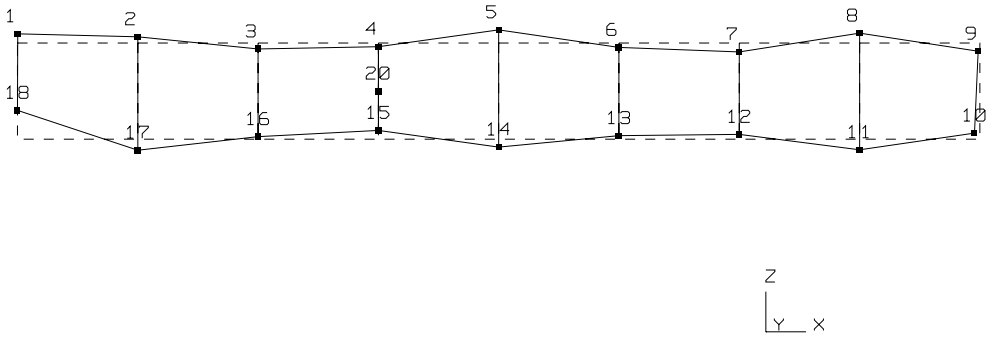

Fig. 10n. 5th Breathing Mode of Tube 3 (Mode 5BR)

FREQUENCY, HZ = 2600 CMI, % = 62.75
DAMPING, % = 1.395 MPC, % = 77.54

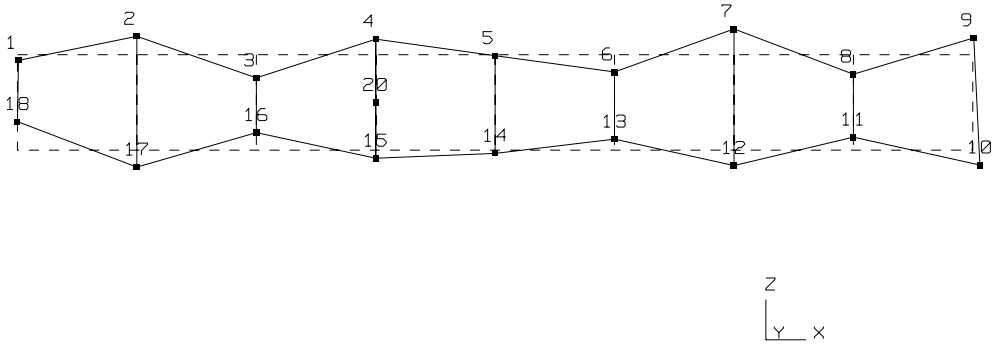

Fig. 10o. 6th Breathing Mode of Tube 3 (Mode 6BR)

FREQUENCY, HZ = 433 CMI, % = 98.62
DAMPING, % = 0.320 MPC, % = 99.64

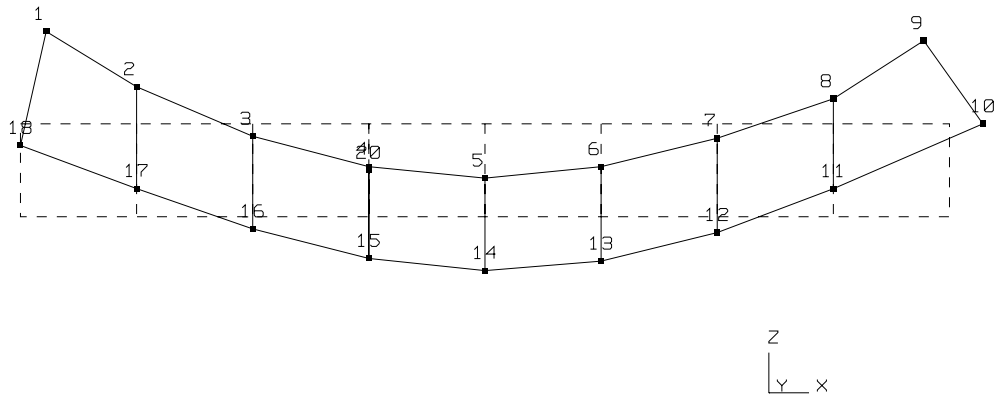

Fig. 11a. 1st Bending Mode of Tube 4 (Mode 1B-Z)

FREQUENCY, HZ = 1061 CMI, % = 16.35
DAMPING, % = 1.767 MPC, % = 20.33

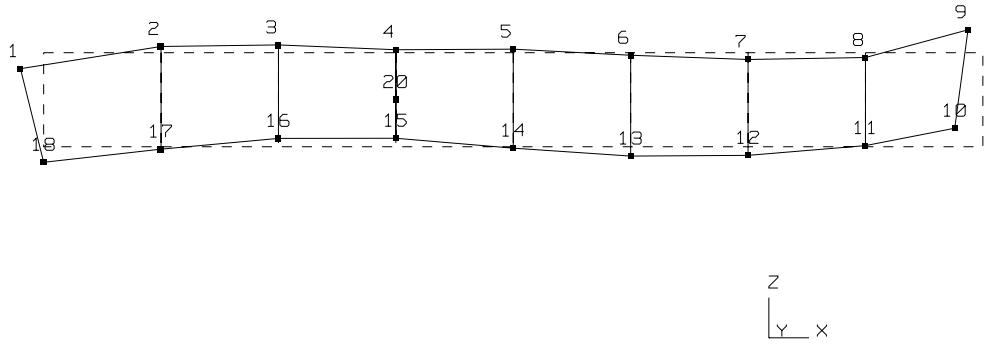

Fig. 11b. 2nd Bending Mode of Tube 4 (Mode 2B-Z)

FREQUENCY, HZ = 1675 CMI, % = 37.83
DAMPING, % = 2.305 MPC, % = 45.79

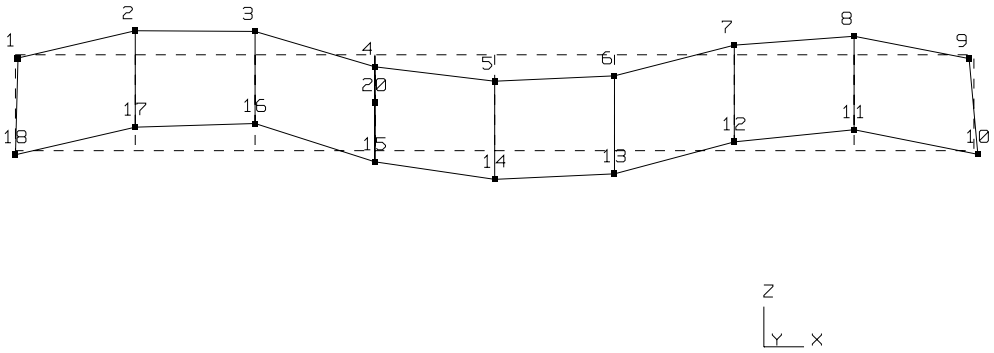

Fig. 11c. 3rd Bending Mode of Tube 4 (Mode 3B-Z)

FREQUENCY, HZ = 1734 CMI, % = 72.30
DAMPING, % = 2.389 MPC, % = 94.23

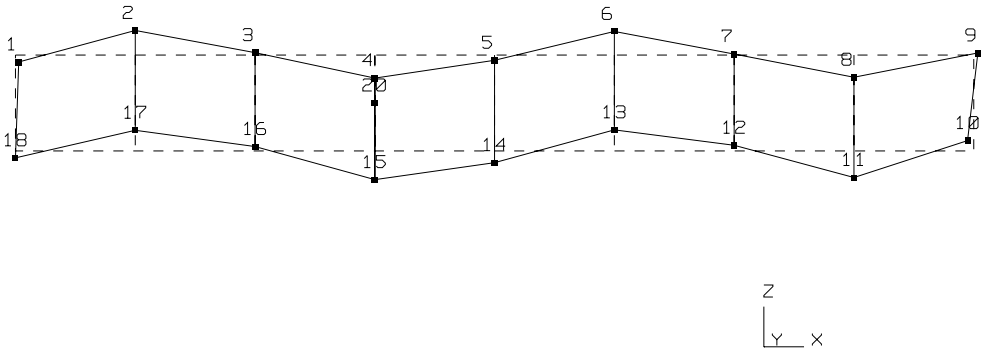

Fig. 11d. 4th Bending Mode of Tube 4 (Mode 4B-Z)

FREQUENCY, HZ = 1865 CMI, % = 52.49
DAMPING, % = 2.390 MPC, % = 90.23

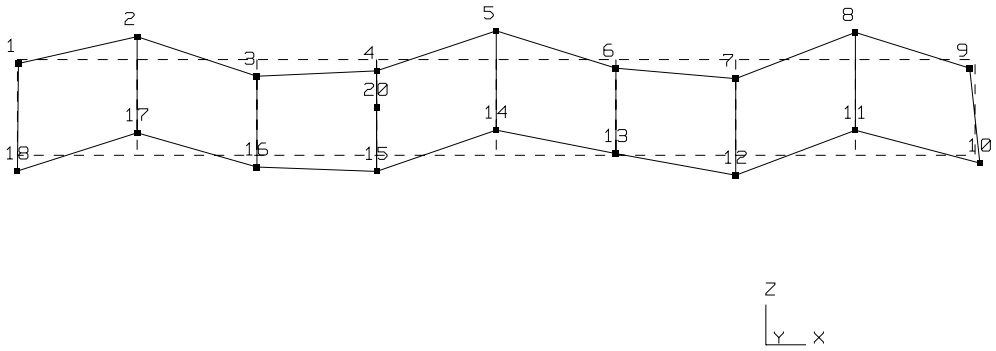

Fig. 11e. 5th Bending Mode of Tube 4 (Mode 5B-Z)

FREQUENCY, HZ = 2037 CMI, % = 85.05
DAMPING, % = 1.858 MPC, % = 96.65

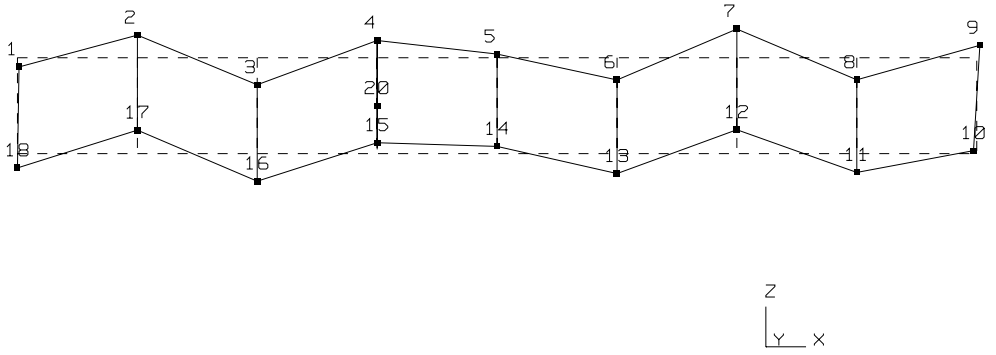

Fig. 11f. 6th Bending Mode of Tube 4 (Mode 6B-Z)

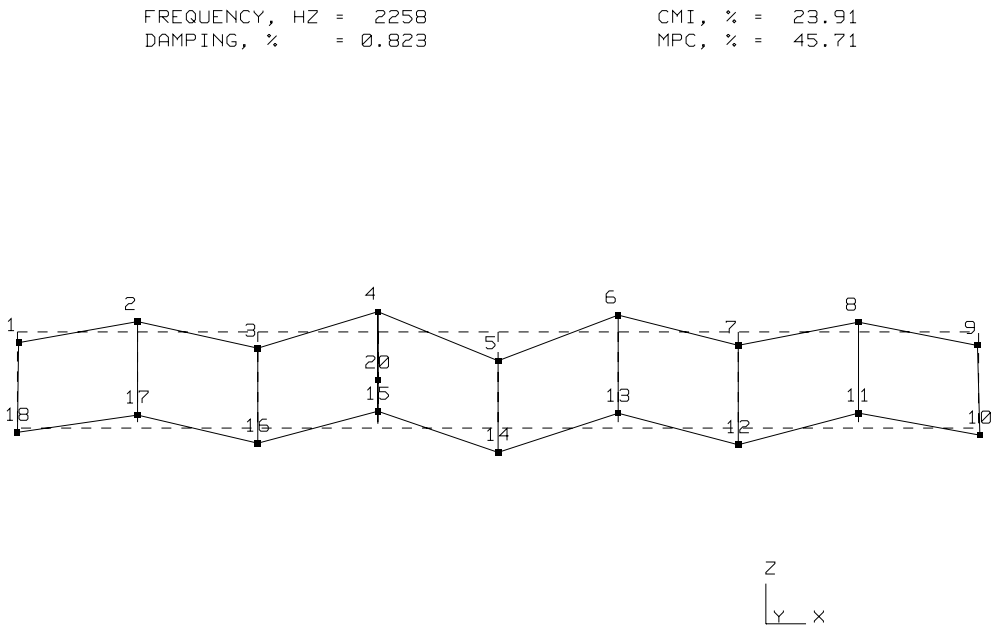

Fig. 11g. 7th Bending Mode of Tube 4 (Mode 7B-Z)

FREQUENCY, HZ = 560 CMI, % = 47.72
DAMPING, % = 3.532 MPC, % = 92.16

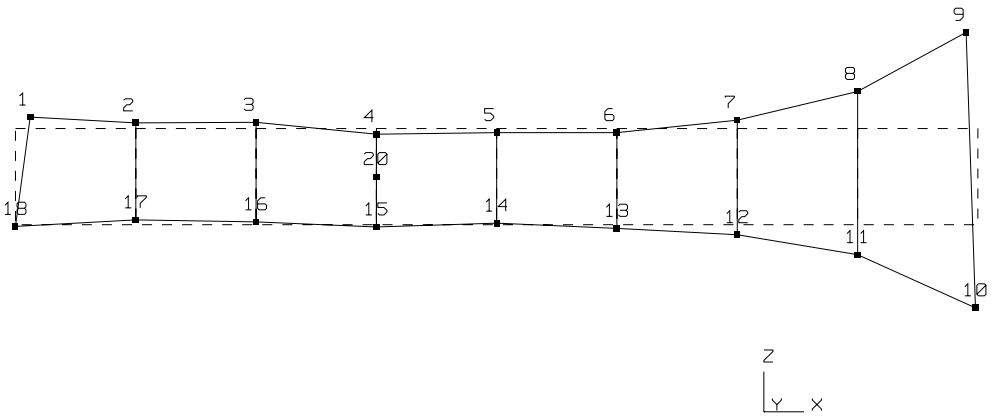

Fig. 11h. Rightside Love Mode of Tube 4 (Mode R-Love)

FREQUENCY, HZ = 659 CMI, % = 34.46
DAMPING, % = 2.990 MPC, % = 83.09

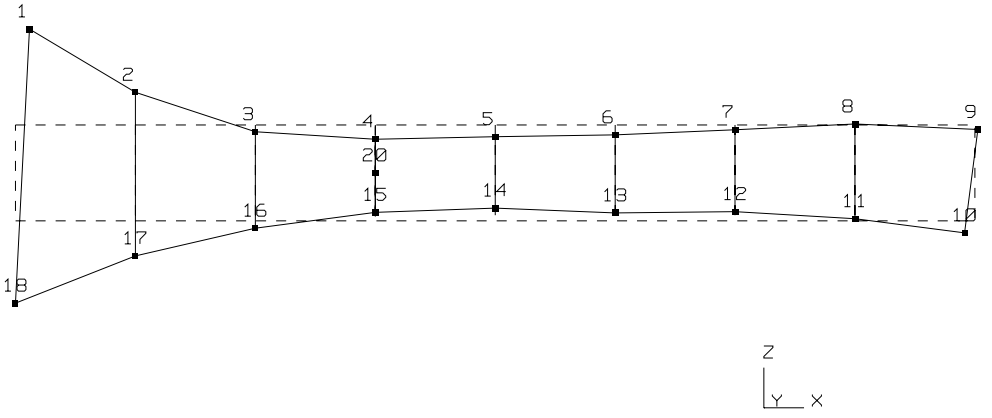

Fig. 11i. Leftside Love Mode of Tube 4 (Mode L-Love)

FREQUENCY, HZ = 712 CMI, % = 82.28
DAMPING, % = 2.167 MPC, % = 96.69

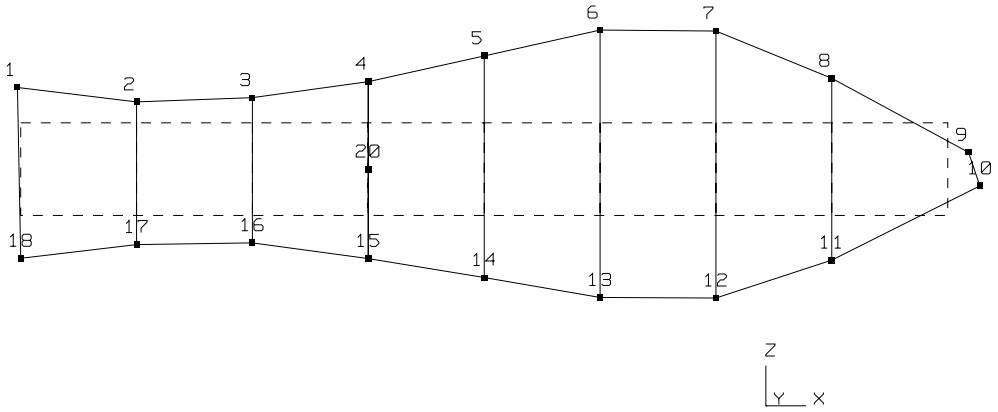

Fig. 11j. 1st Breathing Mode of Tube 4 (Mode 1BR)

FREQUENCY, HZ = 778 CMI, % = 95.31
DAMPING, % = 1.808 MPC, % = 98.55

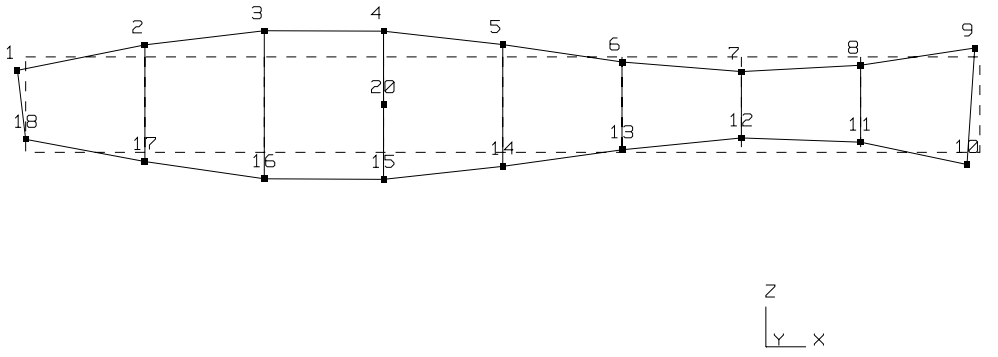

Fig. 11k. 2nd Breathing Mode of Tube 4 (Mode 2BR)

FREQUENCY, HZ = 989 CMI, % = 48.37
DAMPING, % = 2.878 MPC, % = 53.96

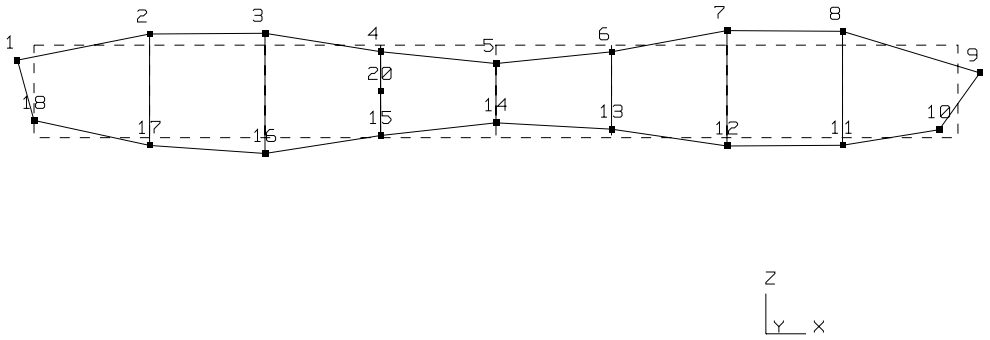

Fig. 11l. 3rd Breathing Mode of Tube 4 (Mode 3BR)

FREQUENCY, HZ = 1332 CMI, % = 70.53
DAMPING, % = 2.055 MPC, % = 77.54

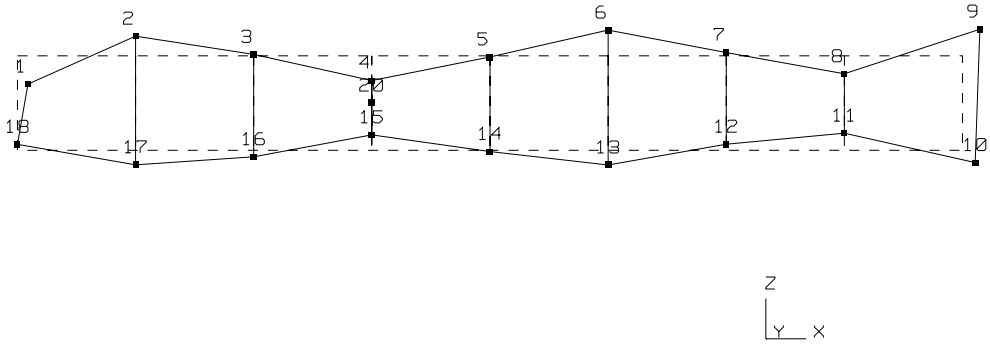

Fig. 11m. 4th Breathing Mode of Tube 4 (Mode 4BR)

FREQUENCY, HZ = 1789 CMI, % = 57.92
DAMPING, % = 2.080 MPC, % = 77.81

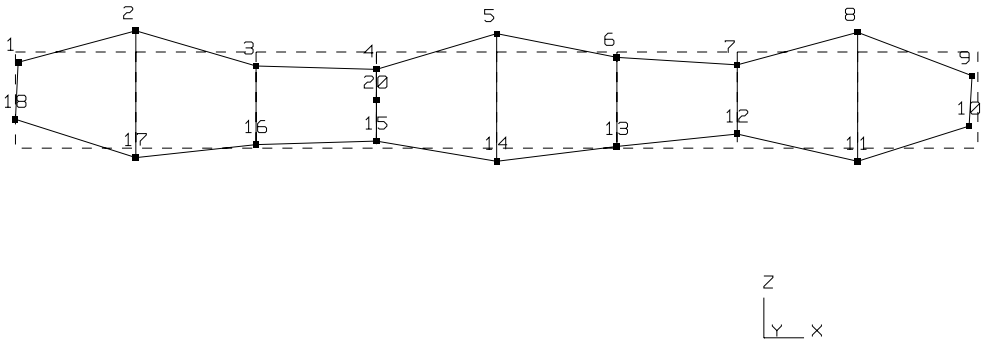

Fig. 11n. 5th Breathing Mode of Tube 4 (Mode 5BR)

FREQUENCY, HZ = 1969 CMI, % = 72.59
DAMPING, % = 2.108 MPC, % = 95.86

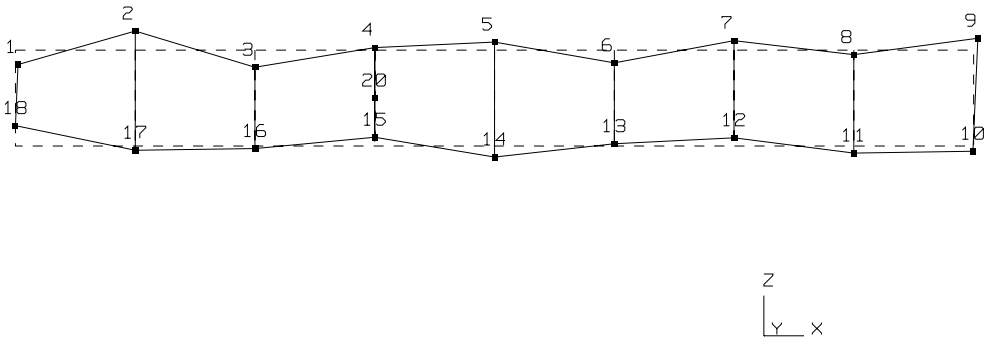

Fig. 11o. 6th Breathing Mode of Tube 4 (Mode 6BR)

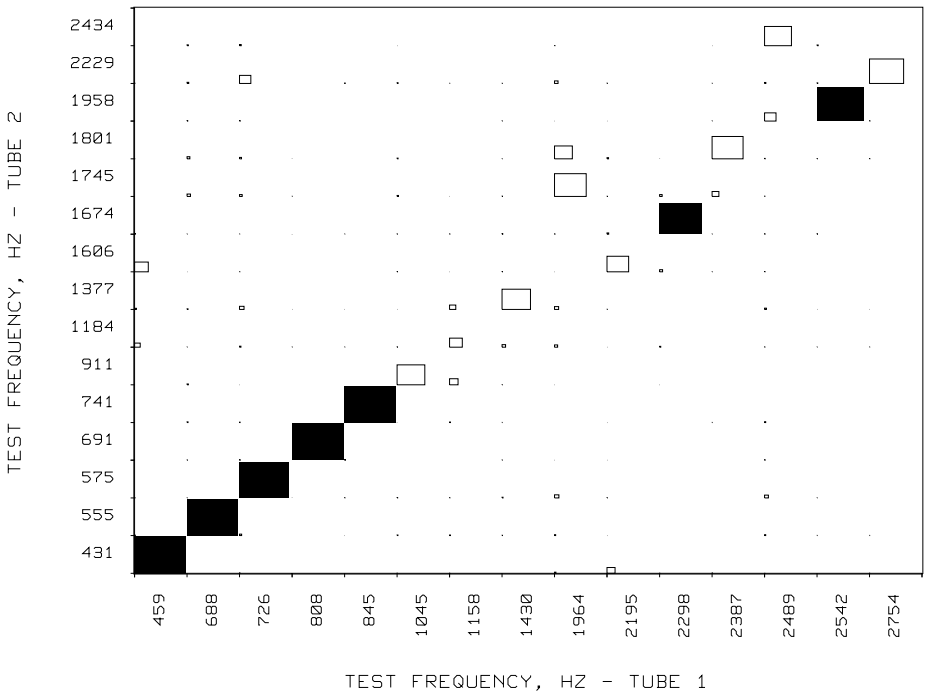

Fig. 12a. Correlation of Tube 1 and Tube 2 Mode Shapes

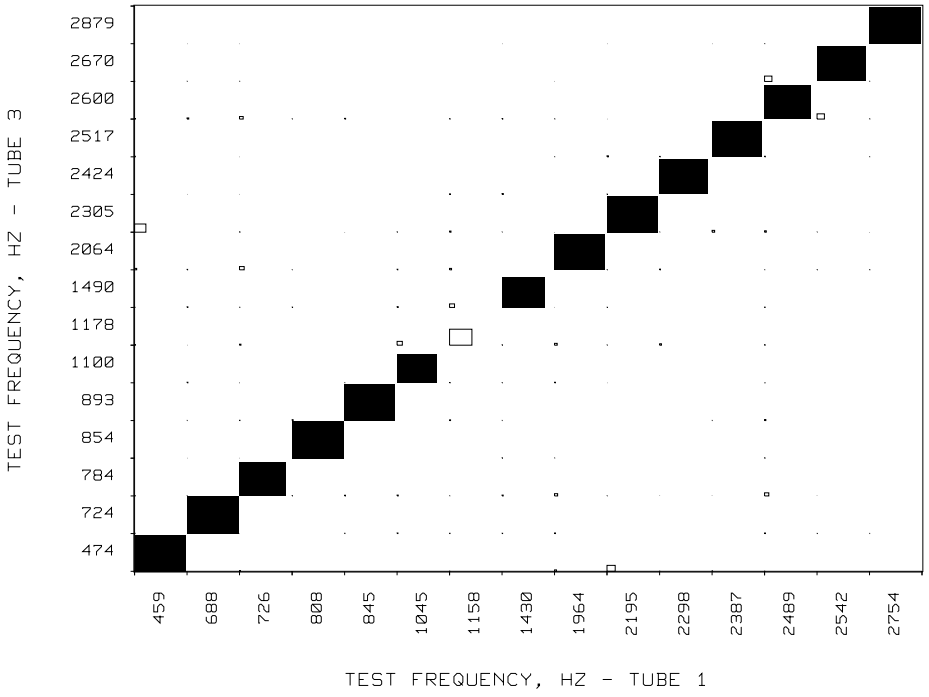

Fig. 12b. Correlation of Tube 1 and Tube 3 Mode Shapes

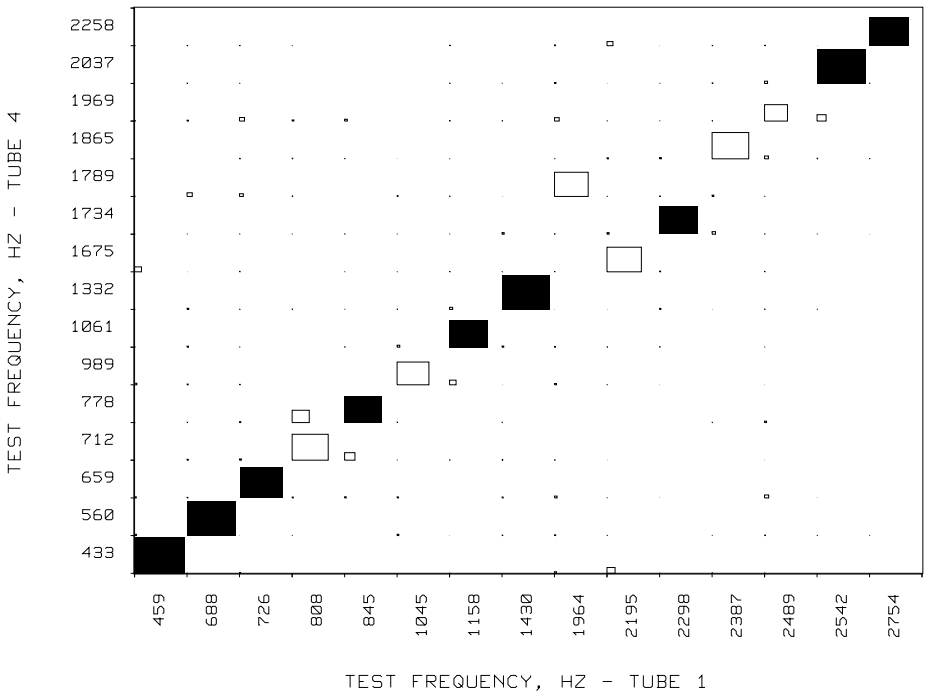

Fig. 12c. Correlation of Tube 1 and Tube 4 Mode Shapes

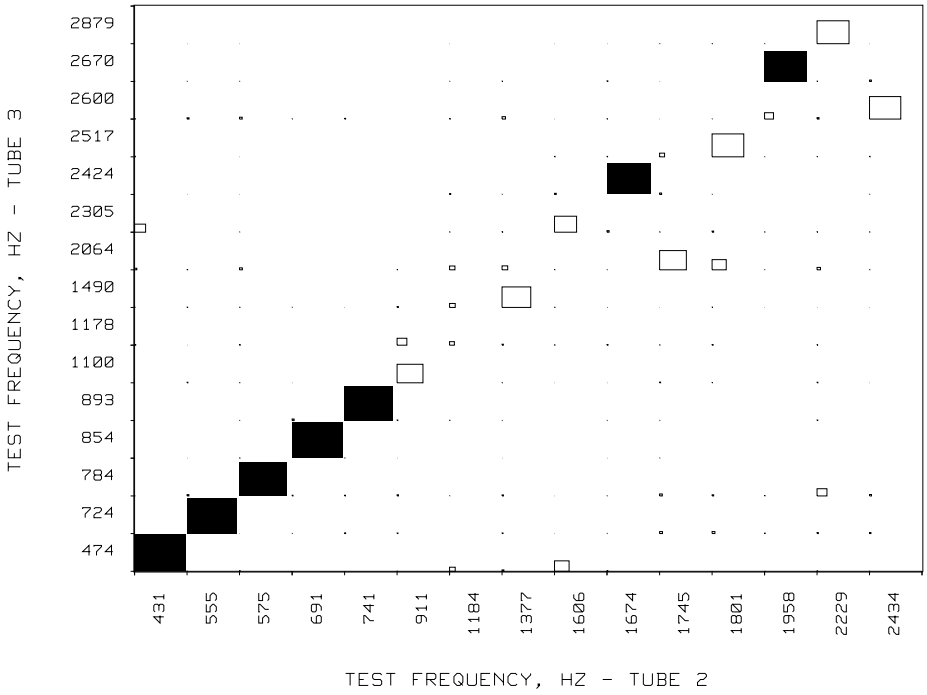

Fig. 12d. Correlation of Tube 2 and Tube 3 Mode Shapes

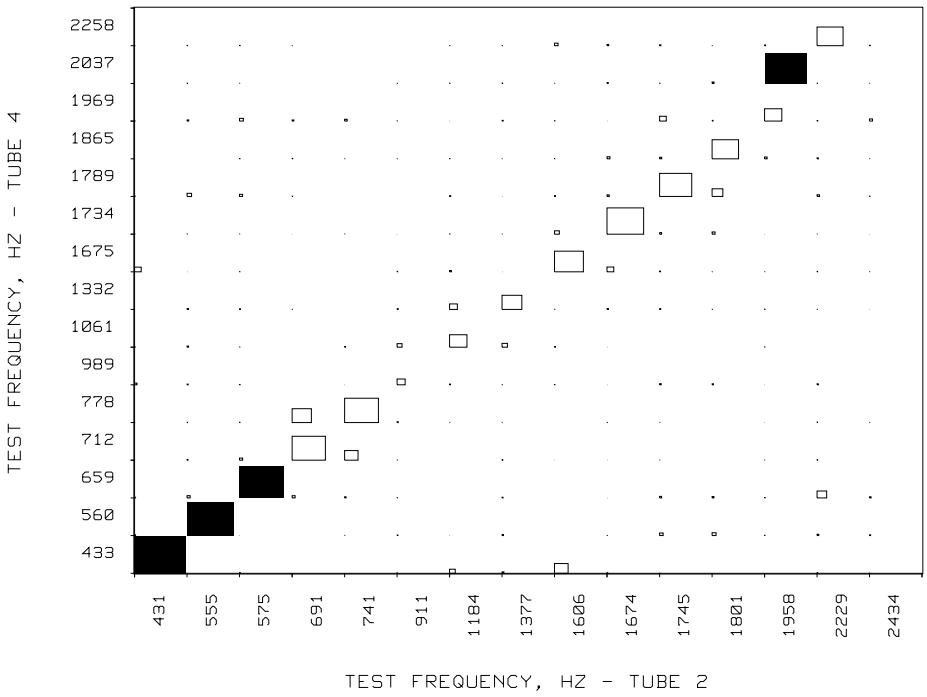

Fig. 12e. Correlation of Tube 2 and Tube 4 Mode Shapes

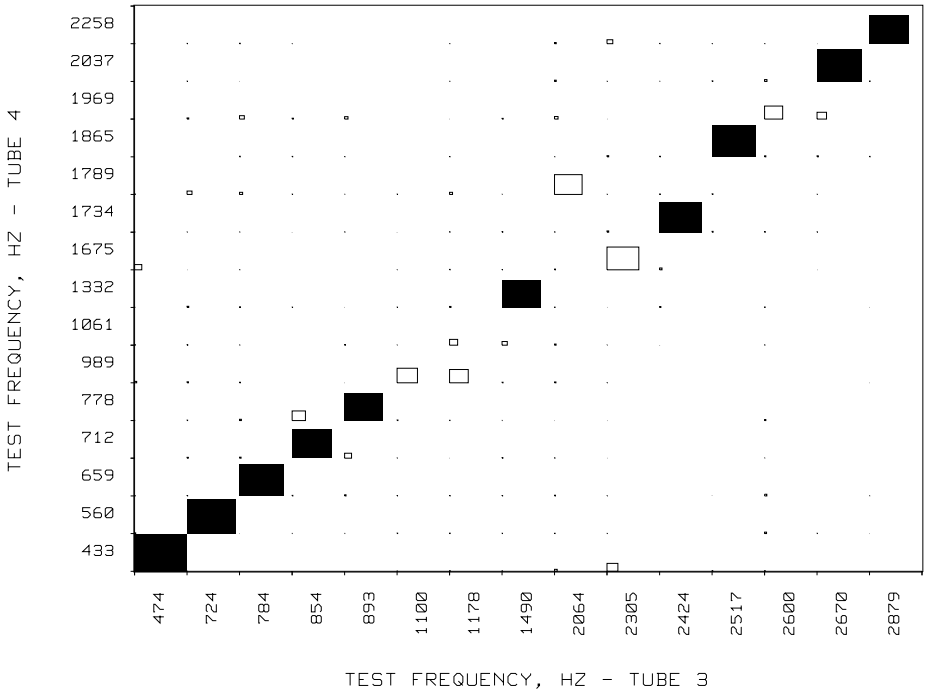

Fig. 12f. Correlation of Tube 3 and Tube 4 Mode Shapes

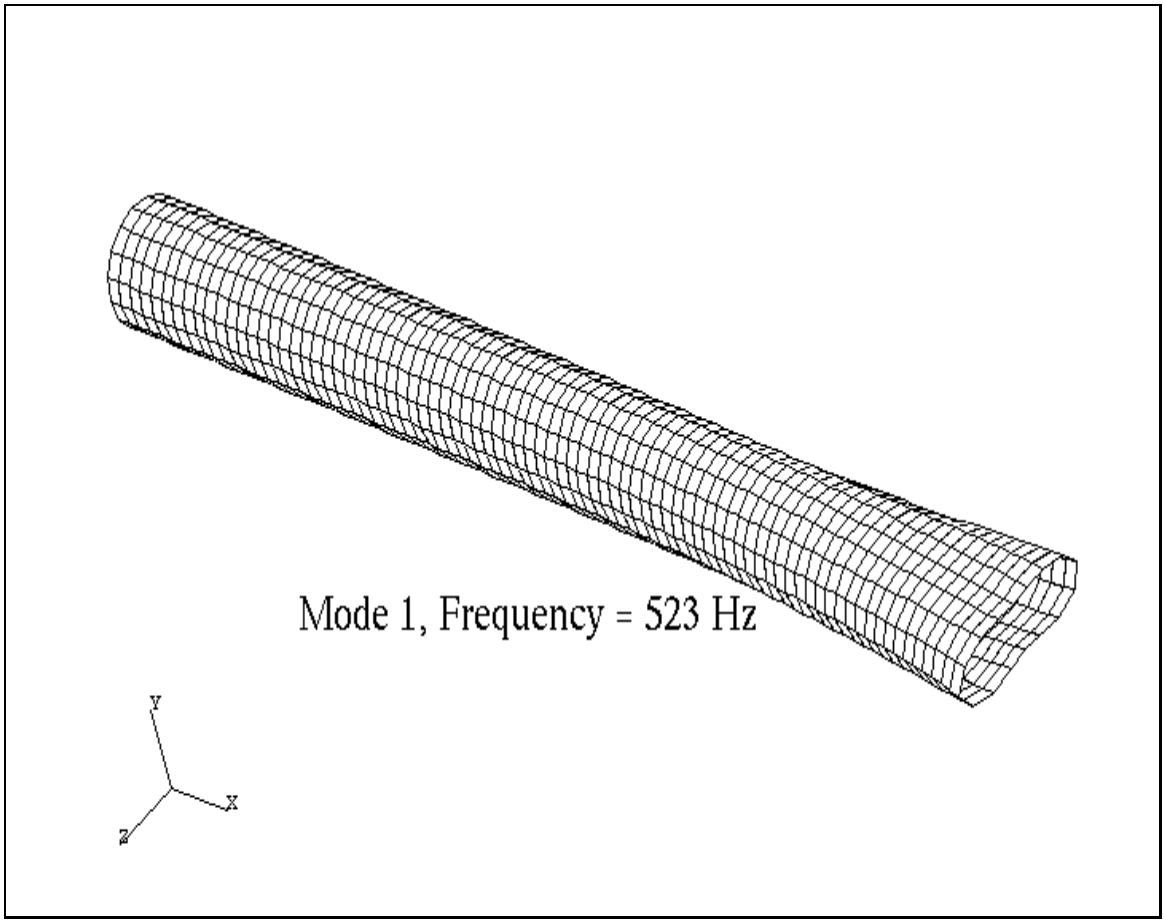

Figure 13a - Computed Right side Love Mode for
tubes 1 and 3 (Frequency = 523 Hz)

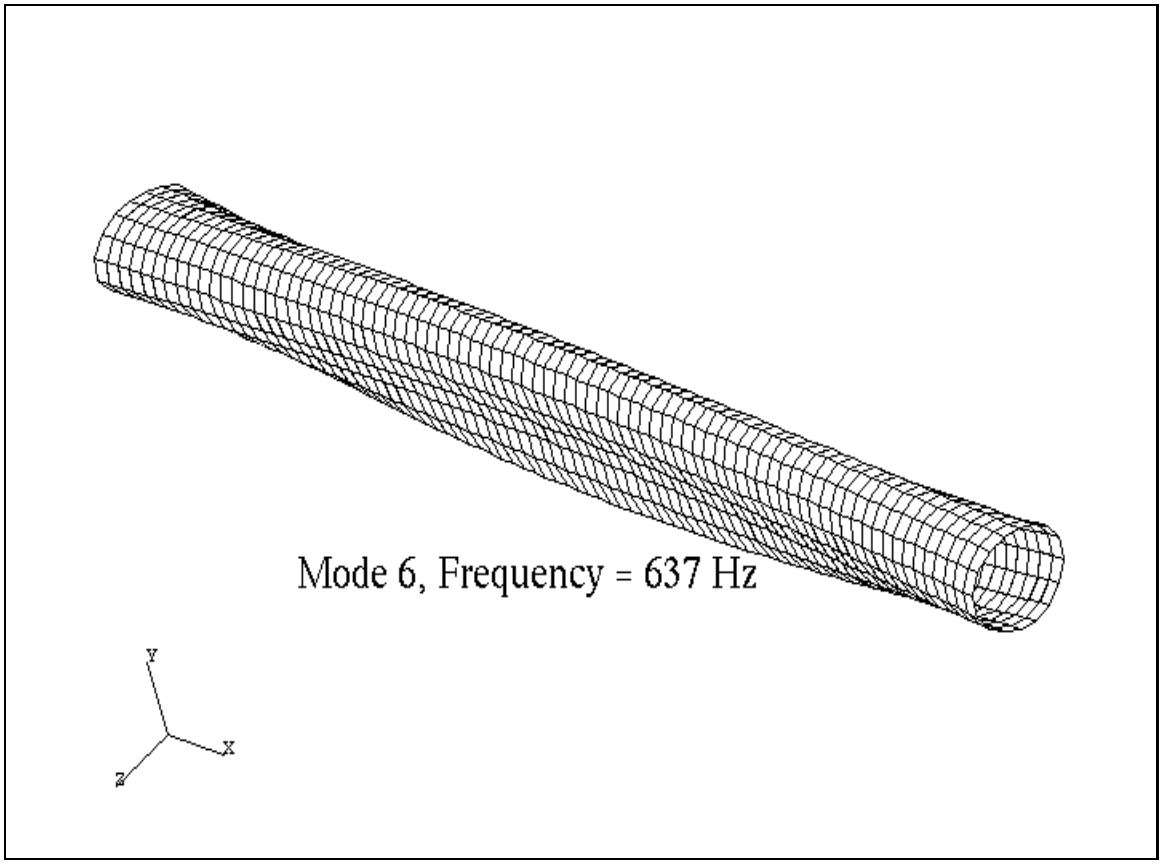

Figure 13b - Computed 1st Breathing Mode for
tubes 1 and 3 (Frequency = 637 Hz)

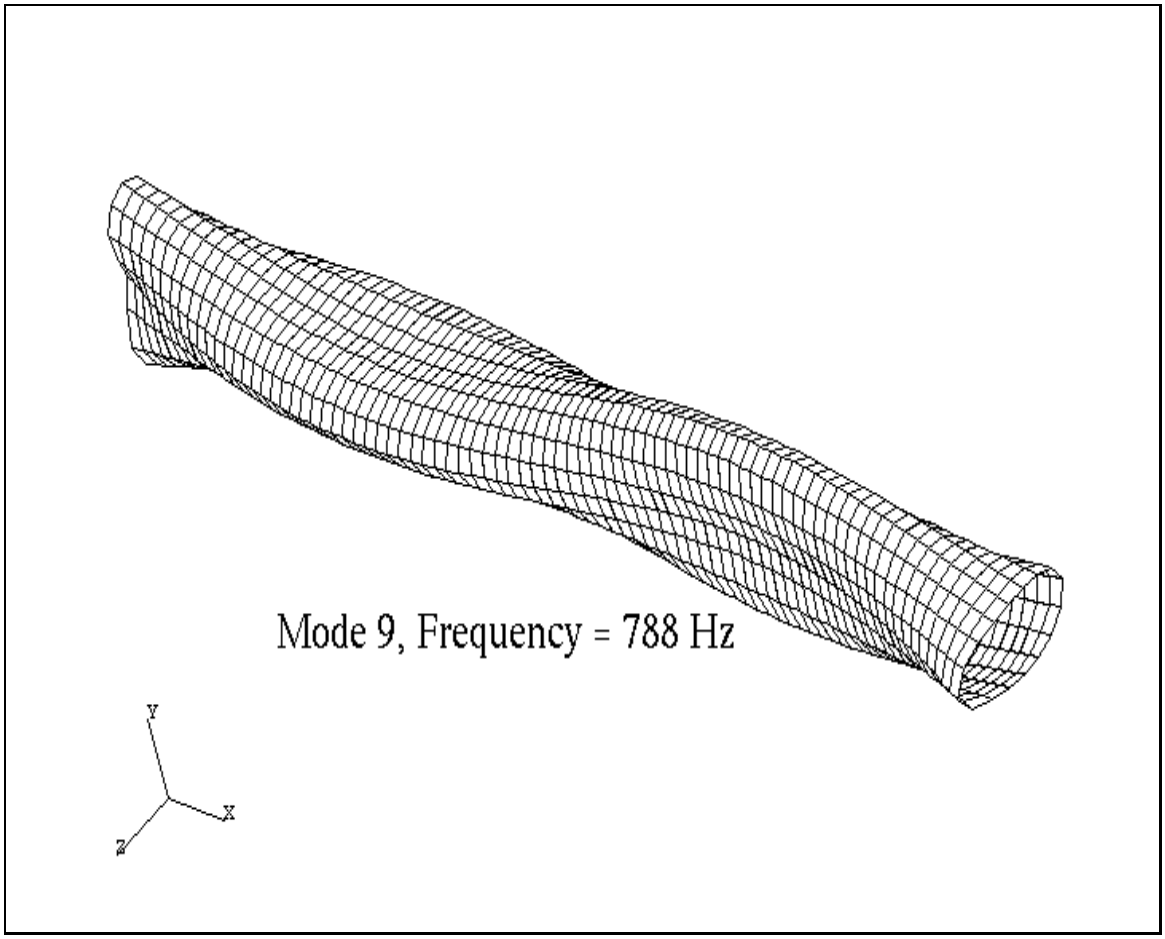

Figure 13c - Computed 2nd Breathing Mode for tubes 1 and 3 (Frequency = 788 Hz)

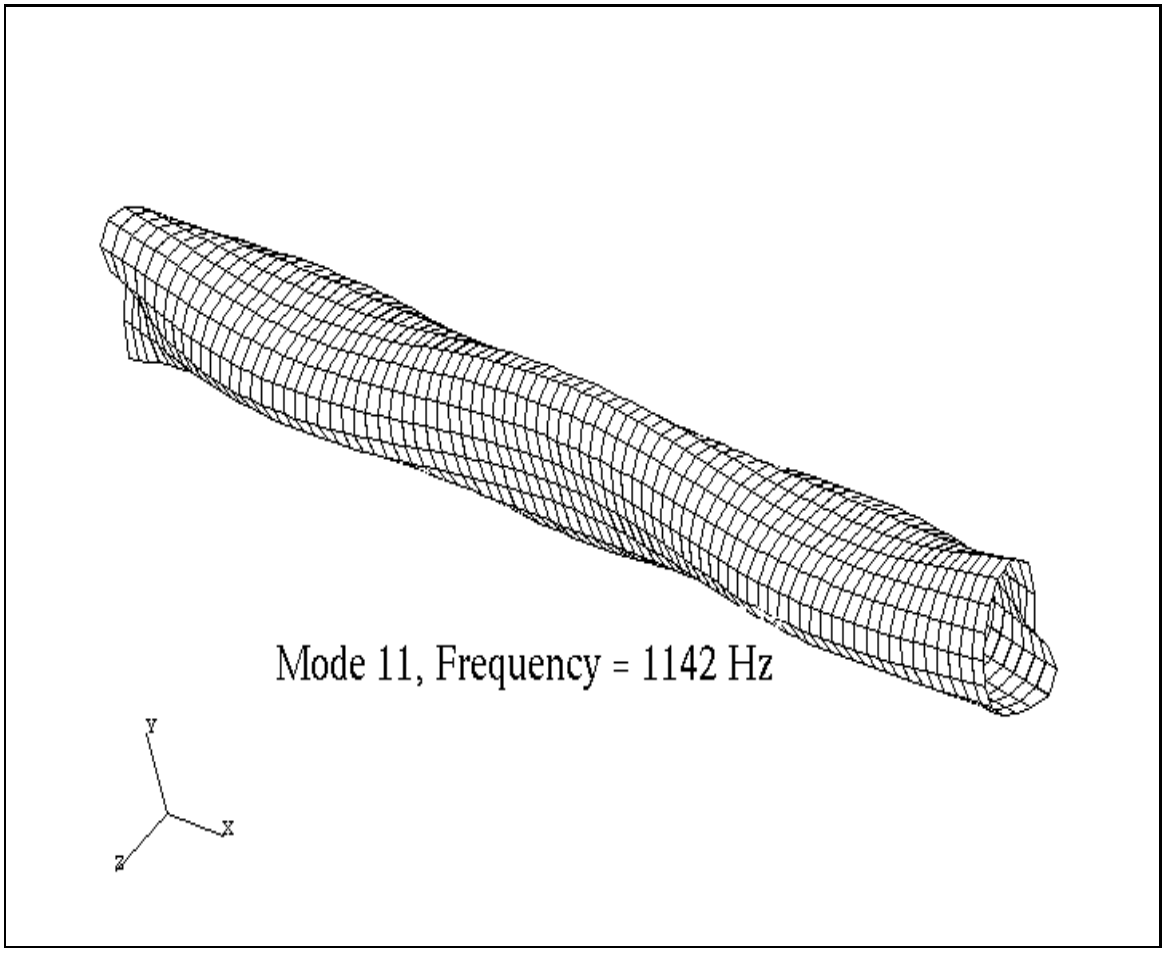

Figure 13d - Computed 3rd Breathing Mode for
tubes 1 and 3 (Frequency = 1142 Hz)

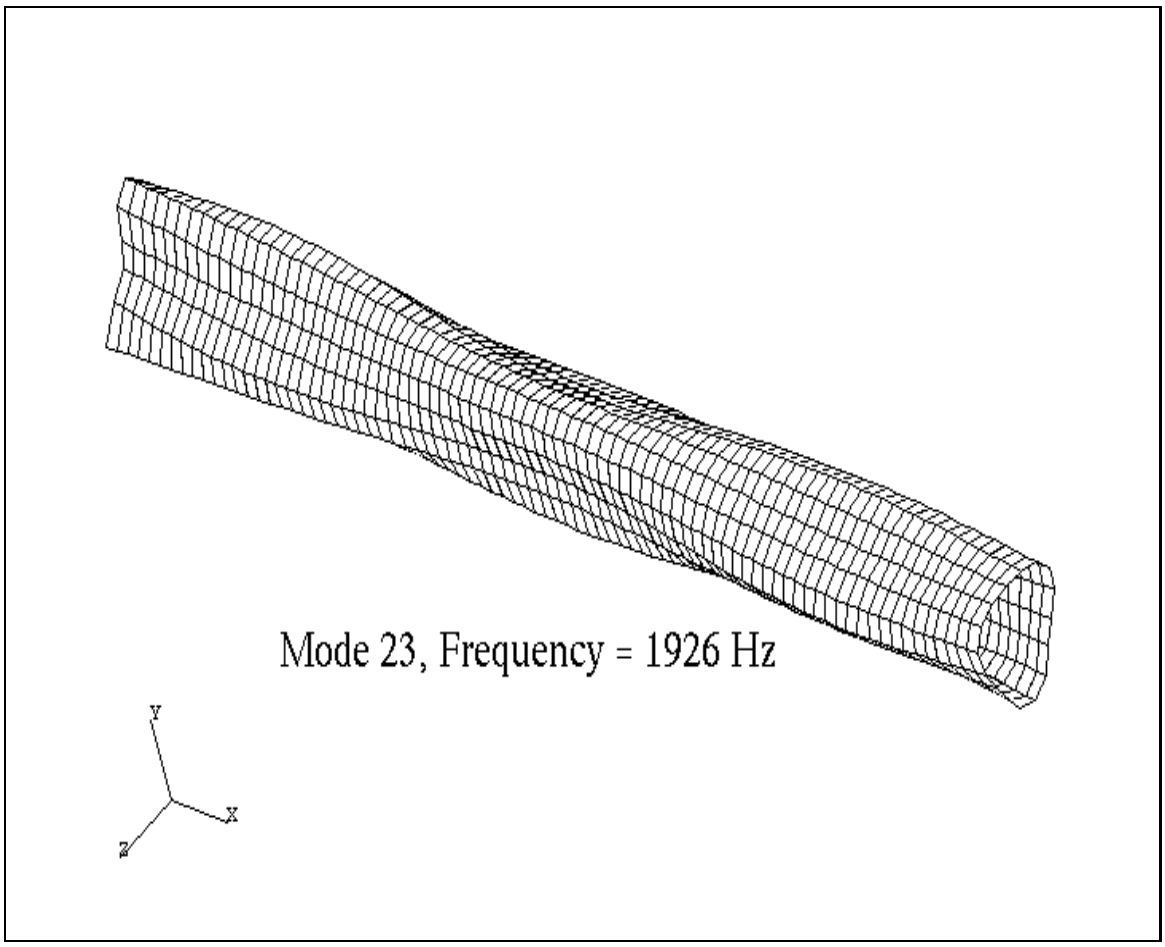

Figure 13e- Computed 3rd Bending Mode
for tube 3 (Frequency = 1926 Hz)

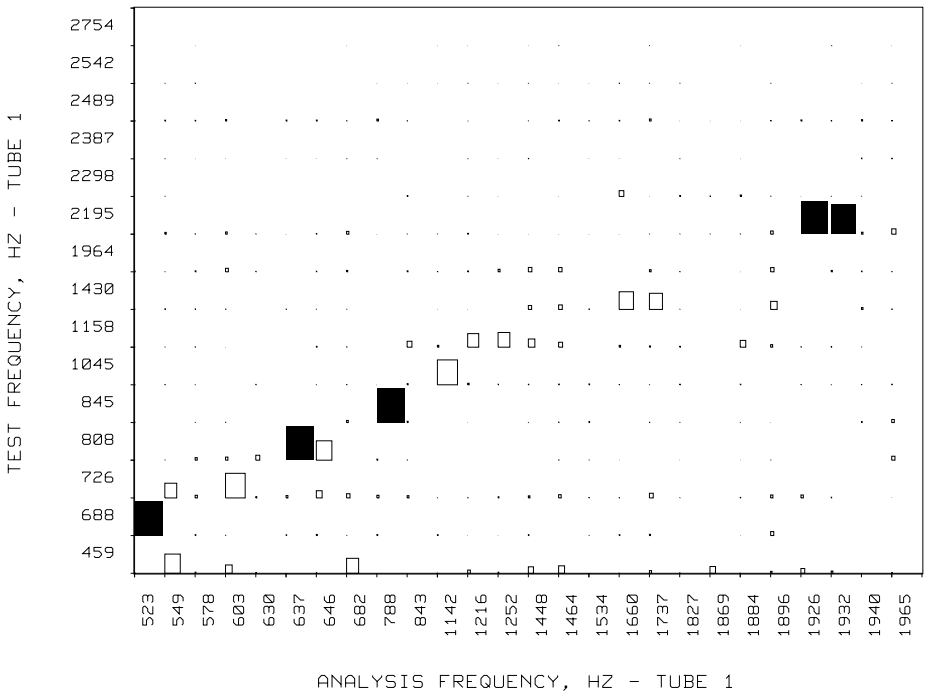

14a Test - Analysis Correlation for Tube 1

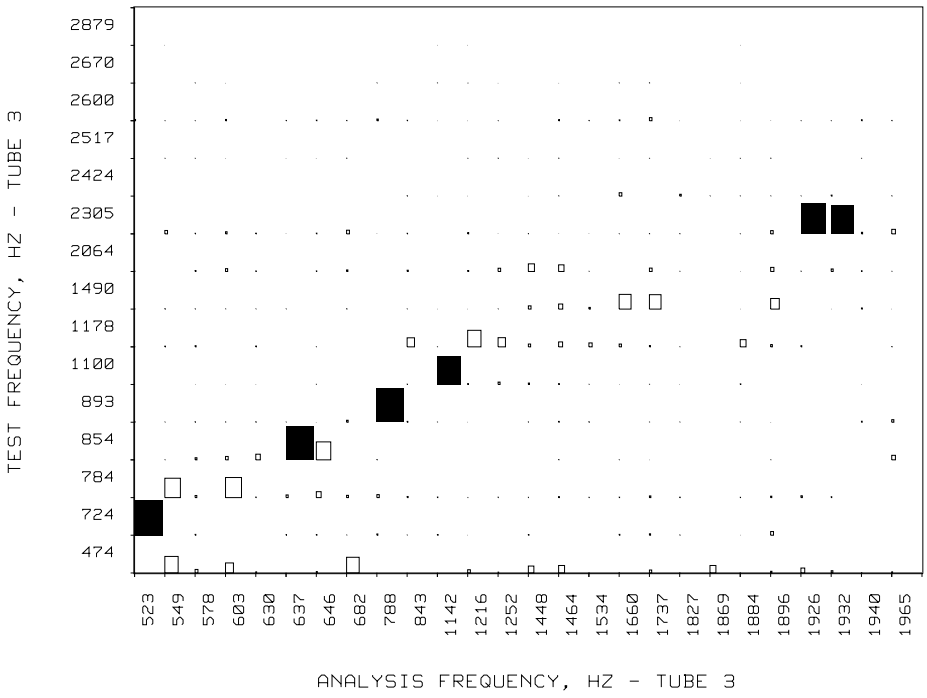

14b Test - Analysis Correlation for Tube 3

Figure 14. Modal Assurance Criterias for tube1 and 3